

Numerical Study of Liquid Crystal Elastomer Using Mixed Finite Element Method

Chong Luo and Maria-Carme Calderer
 School of Mathematics
 University of Minnesota
 Minneapolis, MN 55455

March 13, 2022

Abstract

We aimed to use finite element method to simulate the unique behaviors of liquid crystal elastomer, such as semi-soft elasticity, stripe domain instabilities etc. We started from an energy functional with the 2D Bladon-Warner-Terentjev stored energy of elastomer, the Oseen-Frank energy of liquid crystals, plus the penalty terms for the incompressibility constraint on the displacement, and the unity constraint on the director. Then we applied variational principles to get the differential equations. Next we used mixed finite element method to do the numerical simulation. The existence, uniqueness, well-posedness and convergence of the numerical methods were investigated. The semi-soft elasticity was observed, and can be related to the rotation of the directors. The stripe domain phenomenon, however, wasn't observed. This might due to the relative coarse mesh we have used.

1 Introduction

Nematic liquid crystal elastomer is a relatively new kind of elastic material which combines properties from both incompressible elasticity and rod-like liquid crystals. It has some unique behaviors such as the stripe-domain phenomenon and the semi-soft elasticity. These phenomena are usually observed in the “clamped-pulling” experiment, in which a piece of rectangular shape liquid crystal elastomer is clamped at two ends and pulled along the direction perpendicular to the initial alignment of the directors.

Mitchell et al. [17] did the “clamped-pulling” experiment for *acrylate-based* monodomain networks. They found that the directors rotate in a discontinuous way: after a critical strain, the directors switch to the direction perpendicular to the original alignment. On the other hand, Kundler and Finkelmann [13] did the same experiment for *polysiloxane* liquid crystal elastomer. They found that the directors rotate in a continuous manner. They also observed the interesting stripe domain phenomenon. Later, Zubarev and Finkelmann [20] re-investigated the “clamped-pulling” experiment for polysiloxane liquid crystal elastomers, to investigate the role of aspect ratio of the rectangular shape monodomain in the formation of stripe domains. Figure 1 shows the process of the “clamped-pulling” experiment in the case that the aspect ratio is $AR = 1$. In this graph, the pulling direction is vertical, while the initial alignment of the directors is horizontal. The size of the elastomer was $5 \times 5mm^2$, with thickness $50 - 300 \pm 5 \mu m$. They found that at some critical elongation factor $\lambda = 1.1$, an opaque region started to emerge in the center of the elastomer. Using X-rays, they found that this region was made of stripes of about $15\mu m$ in width. In each stripe, the directors were aligned uniformly, while across the stripes, the directors were aligned in a zig-zag way, as shown in the second picture of Figure 1. When the elastomer was pulled further, the opaque region was broken into two regions symmetric about the center (the

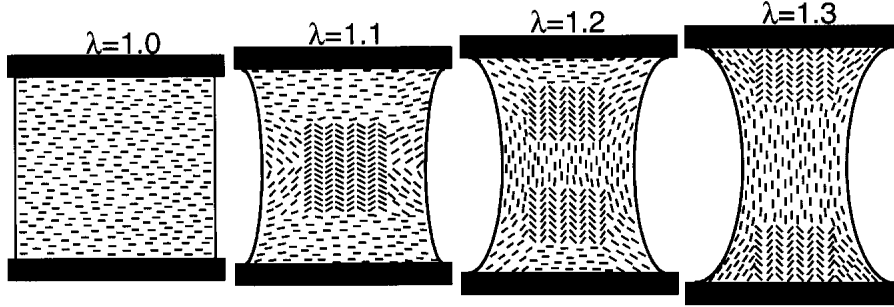


Figure 1: The stripe domain phenomenon. Reproduced from [20]

third picture of Figure 1). And these two regions moved closer to the two ends as the elastomer was pulled further. Eventually at $\lambda = 1.3$ the two stripe domain regions reached the two ends (the last picture of Figure 1) and in this last stage, most of the directors at the center had rotated 90 degrees, and were now aligned in the pulling direction (vertical direction).

Another interesting phenomenon of liquid crystal elastomers is the so-called “semi-soft elasticity”. Figure 2 shows the stress-strain graph of three different kinds of liquid crystal elastomers

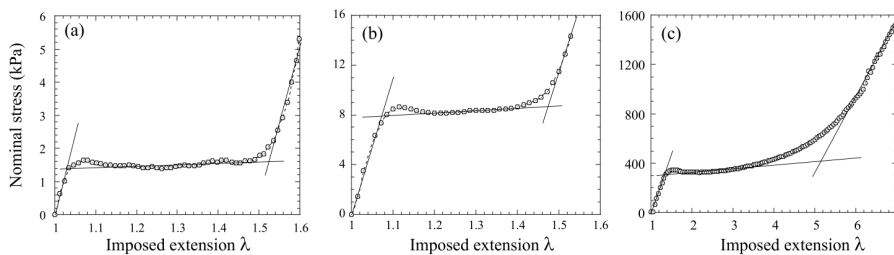


Figure 2: The semi-softness of liquid crystal elastomer. Reproduced from [19].

in the “clamped-pulling” experiment ([14, 7]). We can see that at the beginning, the nominal stress increases linearly with the strain, just like ordinary elastic materials. However, after the strain reaches a critical point, the stress-strain curve becomes relatively “flat”, which we call the “plateau region”. When the strain falls in this region, relatively small stress can induce relatively large deformation, which means the elastomer is “soft”. We can also see from Figure 2 that when the strain continues to increase and reaches another critical value, the stress-strain curve becomes linear again.

The stored energy of liquid crystal elastomer proposed by Bladon, Warner and Terentjev (BTW) is [2]

$$W(F, \mathbf{n}) = \mu \left(|F|^2 - (1 - a)|F^T \mathbf{n}|^2 - 3a^{1/3} \right) \quad (1)$$

where $F = I + \nabla \mathbf{u}(\mathbf{X})$ is the deformation gradient of the elastomer network, while $\mathbf{n} = \mathbf{n}(\mathbf{X})$ is a unit vector denoting the orientation of the rod-like liquid crystal polymers, and \mathbf{X} denotes an arbitrary point in the reference configuration. We assume that the elastomer is incompressible, which is equivalent to $\det(F) = 1$. Also μ is the elasticity constant, and $a \in (0, 1)$ is a constant measuring the significance of the interaction between the displacement \mathbf{u} and the orientation \mathbf{n} . Notice that in the limit $a = 1$, the BTW energy degenerates to the stored energy of incompressible neo-Hookean materials. The closer the value a is to 1, the smaller the interaction between the displacement \mathbf{u} and the orientation \mathbf{n} . Similarly in 2D, the BTW energy can be defined as

$$W(F, \mathbf{n}) = \mu \left(|F|^2 - (1 - a)|F^T \mathbf{n}|^2 - 2a^{1/2} \right) \quad (2)$$

The only difference is that the constant term is changed from $3a^{1/3}$ to $2a^{1/2}$.

Proposition 1. *The BTW energy $W(F, \mathbf{n})$ in equation (1) and (2) are always non-negative.*

- In 3D, $W(F, \mathbf{n}) = 0$ if and only if $\text{eig}(FF^T) = \{a^{1/3}, a^{1/3}, a^{-2/3}\}$ and \mathbf{n} is an eigenvector of the eigenvalue $a^{-2/3}$.
- In 2D, $W(F, \mathbf{n}) = 0$ if and only if $\text{eig}(FF^T) = \{a^{1/2}, a^{-1/2}\}$ and \mathbf{n} is an eigenvector of the eigenvalue $a^{-1/2}$.

Proposition 2. • In 3D, assume $\lambda(t) = \lambda(t) = a^{1/6}(1-t) + a^{-1/3}t$ with $0 \leq t \leq 1$. When there is no shearing and

$$F = \begin{pmatrix} a^{1/6} & 0 & 0 \\ 0 & \lambda(t) & 0 \\ 0 & 0 & a^{-1/6}/\lambda(t) \end{pmatrix} \quad (3)$$

the BTW energy (1) is zero for $t = 0, 1$ and strictly positive for $0 < t < 1$. However, when there is shearing and

$$F = \begin{pmatrix} a^{1/6} & 0 & 0 \\ 0 & \lambda(t) & \pm\delta \\ 0 & 0 & a^{-1/6}/\lambda(t) \end{pmatrix} \quad (4)$$

with

$$\delta = \sqrt{a^{1/3} + a^{-2/3} - (\lambda^2 + a^{-1/3}/\lambda^2)}, \quad (5)$$

the BTW energy (1) can be zero for $0 \leq t \leq 1$.

- In 2D, assume $\lambda(t) = a^{1/4}(1-t) + a^{-1/4}t$ with $0 \leq t \leq 1$. When there is no shearing and

$$F = \begin{pmatrix} \lambda(t) & 0 \\ 0 & 1/\lambda(t) \end{pmatrix} \quad (6)$$

the BTW energy (2) is zero for $t = 0, 1$ and is strictly positive for $0 < t < 1$. However, when there is shearing and

$$F = \begin{pmatrix} \lambda(t) & \pm\delta \\ 0 & 1/\lambda(t) \end{pmatrix} \quad (7)$$

with

$$\delta = \sqrt{a^{1/2} + a^{-1/2} - (\lambda^2 + \lambda^{-2})}, \quad (8)$$

the BTW energy (2) can be zero for $0 \leq t \leq 1$.

Corollary 3. *If we take*

$$W(F) = \min_{|\mathbf{n}|=1} W_{BTW}(\mathbf{n}, F), \quad (9)$$

$$= \begin{cases} \mu (\lambda_1^2 + \lambda_2^2 + a\lambda_3^2 - 3a^{1/3}) & \text{in 3D} \\ \mu (\lambda_1^2 + a\lambda_2^2 - 2a^{1/2}) & \text{in 2D} \end{cases} \quad (10)$$

then $W(F)$ is a non-convex function of F .

Proof. Take $0 < t < 1$, and $\lambda(t)$ and F_{\pm} as defined Proposition 2. Then we have

$$W(0.5F_+ + 0.5F_-) > 0$$

while

$$0.5W(F_+) + 0.5W(F_-) = 0$$

Therefore $W(F)$ is a non-convex function of F . □

Proposition 2 tells us that introducing shearing might lower the BTW energy (1) or (2). On the other hand, because of the constraint of the clamps, global shearing is not possible, therefore, local shearing is developed in a zig-zag way, and that’s why stripe domains occur.

In [8], DeSimone et al. did the finite element study of the clamped pulling of liquid crystal elastomer. They started from the 3D BTW energy (1), and got rid of the variable \mathbf{n} by taking it to be always $\mathbf{n} = \mathbf{n}(F)$, the eigenvector of the largest eigenvalue $a^{-2/3}$ of the matrix FF^T . So they got

$$W(F) = \mu \left(\lambda_1^2(F) + \lambda_2^2(F) + a\lambda_3^2(F) - 3a^{1/3} \right) \quad (11)$$

It turned out that the energy function (11) is no longer a convex function of F (Corollary 3). Therefore, they replaced it by its quasi-convex envelope

$$W_{qc}(F) := \inf_{\substack{y \in W^{1,\infty} \\ \det(\nabla y(x))=1}} \left\{ \frac{1}{|\Omega|} \int_{\Omega} W(\nabla y(x)) dx : y(x) = Fx \text{ on } \partial\Omega \right\} \quad (12)$$

They pointed out, that the use of $W_{qc}(F)$ in the numerical computations allows one to resolve only the *macroscopic* length scale, with the (possibly infinitesimal) microscopic scale already accounted for in $W_{qc}(F)$.

It turned out that their approach was very successful, in that they successfully captured the emerging and migrating of the stripe domain regions, in exactly the same way as those observed experimentally in [20]. However, their approach is limited for several reasons:

- Although they were able to tell which part of the region is a “stripe-domain region”, they couldn’t tell how many stripes lie in that region. Actually, their model permits infinitely many stripes in that region, which is unphysical.
- They were only able to observe the “soft elasticity”, not the “semi-soft elasticity”. That is, the plateau region occurs immediately upon the pulling (Figure 3), instead of after some critical strain as observed experimentally.

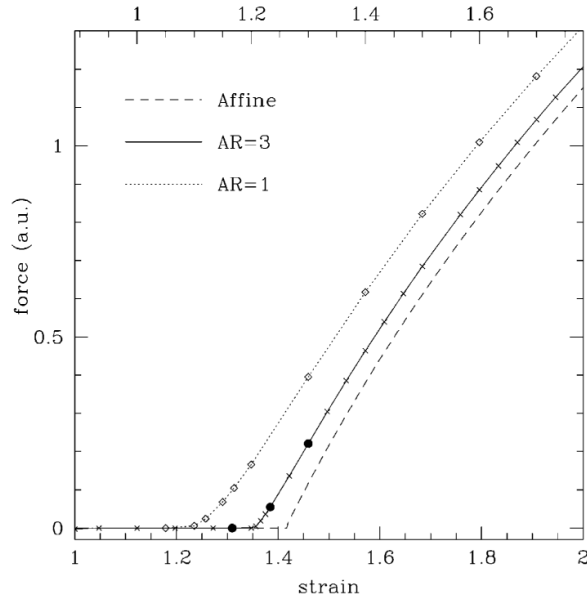


Figure 3: The stress-strain curve from Desimone’s numerical simulation. Soft elasticity instead of semi-soft elasticity was observed. Reproduced from [8].

In this work, we aim to resolve the above issues. We combine the 2D BTW model (2) and the

Oseen-Frank model ([11]), and get the following energy functional for liquid crystal elastomers:

$$\begin{aligned}\Pi(\mathbf{u}, \mathbf{n}) &= \int_{\Omega} c (|F|^2 - (1-a)|F^T \mathbf{n}|^2) + b|\nabla \mathbf{n}|^2 \\ &\quad - \int_{\Omega} \mathbf{f} \cdot \mathbf{u} - \int_{\Gamma_2} \mathbf{g} \cdot \mathbf{u} da\end{aligned}$$

where \mathbf{f} is the body force, while \mathbf{g} is the traction force on the Γ_2 part of the boundary $\partial\Omega$. We assume $\mathbf{u} \in H^1(\Omega)$, and satisfies $\det(I + \nabla \mathbf{u}) = 1$ a.e. in Ω ; while $\mathbf{n} \in H^1(\Omega)$, and satisfies $|\mathbf{n}| = 1$ a.e. in Ω . Let L be the characteristic length scale of the domain Ω , we get the following non-dimensionalized energy

$$\begin{aligned}\tilde{\Pi}(\mathbf{u}, \mathbf{n}) &= \int_{\tilde{\Omega}} (|F|^2 - (1-a)|F^T \mathbf{n}|^2) + \tilde{b}|\nabla \mathbf{n}|^2 \\ &\quad - \int_{\tilde{\Omega}} \tilde{\mathbf{f}} \cdot \mathbf{u} - \int_{\tilde{\Gamma}_2} \tilde{\mathbf{g}} \cdot \mathbf{u} da\end{aligned}$$

where $\tilde{\Omega}$ is congruent with Ω with characteristic length scale 1, and $\tilde{\Gamma}_2 \subset \partial\tilde{\Omega}$ is the image of Γ_2 . Also $\tilde{b} = \frac{b}{cL^2}$, $\tilde{\mathbf{f}} = \frac{\mathbf{f}}{cL}$, and $\tilde{\mathbf{g}} = \frac{\mathbf{g}}{c}$.

The rest of the paper is organized as the following. In section 2, we investigated the properties of the continuous problem, such as the existence of minimizer, the equilibrium equation and its linearization, the stress-free state, the well-posedness of the linearized equation etc. In section 3, we investigated problems related to the discretization, such as the existence of minimizer, the equilibrium equation and its linearization, the well-posedness of the linearized equation, and the existence and uniqueness of the Lagrange multipliers etc. In section 4, we presented the simulation results for the ‘‘clamped-pulling’’ experiment, including the results of the inf-sup tests, the convergence rates, and the stress-strain curve etc. Finally, in section 5, we discussed future directions.

2 The Continuous Problem

2.1 Existence of minimizer

Let

$$H^1(\Omega, S^1) = \{\mathbf{n} \in H^1(\Omega, \mathbb{R}^2) : |\mathbf{n}| = 1 \text{ almost everywhere in } \Omega\} \quad (13)$$

and

$$K = \{\mathbf{u} \in H^1(\Omega, \mathbb{R}^2) : \det(I + \nabla \mathbf{u}) = 1 \text{ almost everywhere in } \Omega\} \quad (14)$$

Define the admissible set

$$\mathcal{A}(\mathbf{u}_0, \mathbf{n}_0) = \{\mathbf{u} \in K, \mathbf{n} \in H^1(\Omega, S^1) : \mathbf{u} = \mathbf{u}_0 \text{ on } \Gamma_0, \mathbf{n} = \mathbf{n}_0 \text{ on } \Gamma_1\} \quad (15)$$

Define the energy functional

$$\begin{aligned}\Pi(\mathbf{u}, \mathbf{n}) &= \int_{\Omega} (|F|^2 - (1-a)|F^T \mathbf{n}|^2) + b|\nabla \mathbf{n}|^2 \\ &\quad - \int_{\Omega} \mathbf{f} \cdot \mathbf{u} - \int_{\Gamma_2} \mathbf{g} \cdot \mathbf{u} da\end{aligned} \quad (16)$$

where $F = I + \nabla \mathbf{u}$. Then our problem is

$$\text{Find } (\mathbf{u}, \mathbf{n}) \in \mathcal{A}(\mathbf{u}_0, \mathbf{n}_0) \text{ minimizing } \Pi(\mathbf{u}, \mathbf{n}). \quad (17)$$

Lemma 4. Assume $|\mathbf{n}| = 1$, we have

$$(|F|^2 - (1-a)|F^T \mathbf{n}|^2) \geq a|F|^2 \quad (18)$$

Proof. Let $\lambda_1^2 \leq \lambda_2^2$ be the two eigenvalues of the real symmetric matrix FF^T . Since \mathbf{n} is in $H^1(\Omega, S^1)$, by Proposition 1, we have

$$\begin{aligned} (|F|^2 - (1-a)|F\mathbf{n}|^2) &\geq \lambda_1^2 + a\lambda_2^2 \\ &\geq a(\lambda_1^2 + \lambda_2^2) \\ &= \text{atr}(FF^T) \\ &= a|F|^2 \end{aligned}$$

□

Lemma 5. Assume $|\mathbf{n}| = 1$, and $0 < a < 1$. The function

$$L(F, \mathbf{n}) = |F|^2 - (1-a)|F^T\mathbf{n}|^2 \quad (19)$$

is convex in F .

Proof. Let

$$A(\mathbf{n}) = I - (1-a)\mathbf{n}\mathbf{n}^T \quad (20)$$

Then we have

$$L = \text{tr}(FAF^T) \quad (21)$$

Then for any $F_1, F_2 \in \mathbb{M}^{3 \times 3}$, and $0 \leq \alpha \leq 1$, we have

$$\begin{aligned} &[\alpha L(F_1) + (1-\alpha)L(F_2)] - L(\alpha F_1 + (1-\alpha)F_2) \\ &= \alpha \text{tr}(F_1 A F_1^T) + (1-\alpha) \text{tr}(F_2 A F_2^T) \\ &\quad - \text{tr}[(\alpha F_1 + (1-\alpha)F_2) A (\alpha F_1 + (1-\alpha)F_2)^T] \\ &= \alpha(1-\alpha) \text{tr}[(F_1 - F_2) A (F_1 - F_2)] \\ &= \alpha(1-\alpha) (|F_1 - F_2|^2 - (1-a)|(F_1 - F_2)^T \mathbf{n}|^2) \\ &\geq 2\alpha(1-\alpha)\sqrt{a} \\ &\geq 0 \end{aligned}$$

where we have used Proposition 1. Therefore L is a convex function of F . □

Remark It's easy to see that Lemma 4 and Lemma 5 holds for 3D, too.

Theorem 6. Let Ω be a nonempty, bounded, open subset of \mathbb{R}^d .

- If $d = 2$, suppose we have $\mathbf{u}_k \rightharpoonup \mathbf{u}$ in $W^{1,s}$ with $s > \frac{4}{3}$, then we have $\det(I + \nabla \mathbf{u}_k) \rightarrow \det(I + \nabla \mathbf{u})$ in $\mathcal{D}'(\Omega)$.
- If $d = 3$,
 - suppose we have $\mathbf{u}_k \rightharpoonup \mathbf{u}$ in $W^{1,s}$ with $s > \frac{3}{2}$, then we have $\text{adj}(I + \nabla \mathbf{u}_k)_{ij} \rightarrow \text{adj}(I + \nabla \mathbf{u})_{ij}$ in $\mathcal{D}'(\Omega)$.
 - suppose we have $\mathbf{u}_k \rightharpoonup \mathbf{u}$ in $W^{1,s}$, and $\text{adj}(I + \nabla \mathbf{u}_k) \rightharpoonup \text{adj}(I + \nabla \mathbf{u})$ in $L^q(\Omega; \mathbb{M}^3)$ with $s > 1, q > 1$ and $\frac{1}{s} + \frac{1}{q} < \frac{4}{3}$, then we have $\det(I + \nabla \mathbf{u}_k) \rightarrow \det(I + \nabla \mathbf{u})$ in $\mathcal{D}'(\Omega)$.

For the proof, please see John Ball [1].

Theorem 7. There exists solution to the problem (17).

Proof. Let m be the infimum of Π on $\mathcal{A}(\mathbf{u}_0, \mathbf{n}_0)$, and let $(\mathbf{u}_k, \mathbf{n}_k) \in \mathcal{A}(\mathbf{u}_0, \mathbf{n}_0)$ be a minimizing sequence of Π . Obviously $m < +\infty$. Thus $\Pi(\mathbf{u}_k, \mathbf{n}_k)$ is bounded above. By Lemma 4, we have

$$\begin{aligned} \Pi(\mathbf{u}_k, \mathbf{n}_k) &\geq \int_{\Omega} a|(I + \nabla \mathbf{u}_k)|^2 + b|\nabla \mathbf{n}_k|^2 dx \\ &\quad - \|\mathbf{f}\|_{L^2(\Omega)} \|\mathbf{u}_k\|_{L^2(\Omega)} - \|\mathbf{g}\|_{L^2(\Gamma_2)} \|\mathbf{u}_k\|_{L^2(\Gamma_2)} \\ &\geq \int_{\Omega} a|(I + \nabla \mathbf{u}_k)|^2 + b|\nabla \mathbf{n}_k|^2 dx \\ &\quad - \left(\frac{1}{\varepsilon} \|\mathbf{f}\|_{L^2(\Omega)}^2 + \varepsilon \|\mathbf{u}_k\|_{L^2(\Omega)}^2 \right) - \left(\frac{1}{\varepsilon} \|\mathbf{g}\|_{L^2(\Gamma_2)}^2 + \varepsilon \|\mathbf{u}_k\|_{L^2(\Gamma_2)}^2 \right) \\ &\geq \int_{\Omega} C_1 |(I + \nabla \mathbf{u}_k)|^2 + C_2 |\nabla \mathbf{n}_k|^2 dx - C_3 \end{aligned}$$

where $\varepsilon > 0$ is small and $C_i > 0, i = 1, 2, 3$ are constants and we have applied the generalized Poincaré inequality ([4], p281) and the Trace Theorem ([9], p258) in the last step. Therefore we have $F_k = I + \nabla \mathbf{u}_k$ and $\nabla \mathbf{n}_k$ are bounded in L^2 . Now we have that $\nabla(\mathbf{u}_k - \mathbf{u}_0)$ is bounded in L^2 , by the Poincaré inequality, we have \mathbf{u}_k is bounded in H^1 . On the other hand, since $\nabla \mathbf{n}_k$ is bounded in L^2 and \mathbf{n}_k is in $H^1(\Omega, S^1)$, we can get that \mathbf{n}_k is bounded in H^1 . Now since H^1 is a reflexive Banach space and \mathbf{u}_k and \mathbf{n}_k are bounded in H^1 , we can find a subsequence of \mathbf{u}_k and a subsequence of \mathbf{n}_k such that they are weakly convergent in H^1 . We still denote them as $(\mathbf{u}_k, \mathbf{n}_k)$, and assume $\mathbf{u}_k \rightharpoonup \mathbf{u}, \mathbf{n}_k \rightharpoonup \mathbf{n}$.

Now that $\mathbf{u}_k \rightharpoonup \mathbf{u}$ in H^1 , by Theorem 6, we have $\det(I + \nabla \mathbf{u}_k) \rightarrow \det(I + \nabla \mathbf{u})$ in $\mathcal{D}'(\Omega)$. Since $\det(I + \nabla \mathbf{u}_k) = 1$ a.e., we have $\det(I + \nabla \mathbf{u}) = 1$ a.e. in Ω ¹. On the other hand, weak convergence in H^1 implies strong convergence in L^2 ², thus we can find a subsequence of \mathbf{n}_k that converges point-wise almost everywhere. Therefore we have $|\mathbf{n}| = 1$ almost everywhere. Finally since $\mathbf{u}_k - \mathbf{u}_0 \in H_{0|\Gamma_0}^1$, and $H_{0|\Gamma_0}^1$ is a closed linear subspace of H^1 , by the Mazur's Theorem, it's weakly closed. Therefore $\mathbf{u} - \mathbf{u}_0$ is also in $H_{0|\Gamma_0}^1$, which means $\mathbf{u} = \mathbf{u}_0$ on Γ_0 . Similarly we have $\mathbf{n} = \mathbf{n}_0$ on Γ_1 . Therefore we have $(\mathbf{u}, \mathbf{n}) \in \mathcal{A}(\mathbf{u}_0, \mathbf{n}_0)$.

By Lemma 5, the following function

$$L(F, \mathbf{n}, P) = (|F|^2 - (1 - a)|F^T \mathbf{n}|^2) + b|P|^2$$

is a convex function of F and P . Therefore by Theorem 1 of section 8.2 of [9], Π is weakly lower semi-continuous. Thus we have

$$\begin{aligned} \Pi(\mathbf{u}, \mathbf{n}) &\leq \liminf_{k \rightarrow \infty} \Pi(\mathbf{u}_k, \mathbf{n}_k) \\ &= m \end{aligned}$$

Since m is the infimum of Π on \mathcal{A} , we conclude that

$$\Pi(\mathbf{u}, \mathbf{n}) = m \tag{22}$$

That is, (\mathbf{u}, \mathbf{n}) is the minimizer of Π on \mathcal{A} . □

Remark Theorem 6 is crucial in this existence proof. Since in the 3D case, we need the additional condition that $\text{adj}(F_k)$ is weakly convergent to get the convergence of $\det(F_k)$, the above proof cannot be directly extended to 3D.

¹This is because, by definition, we have

$$\langle \det(I + \nabla \mathbf{u}_k), \phi \rangle \rightarrow \langle \det(I + \nabla \mathbf{u}), \phi \rangle$$

in \mathbb{R} for any $\phi \in \mathcal{D}(\Omega)$. Since $\det(I + \nabla \mathbf{u}_k) = 1$ a.e. in Ω for any k , we have

$$\langle \det(I + \nabla \mathbf{u}) - 1, \phi \rangle = 0, \quad \forall \phi \in \mathcal{D}(\Omega)$$

Thus $\det(I + \nabla \mathbf{u}) = 1$ a.e. in Ω .

²This is because the embedding $I : W^{1,p} \rightarrow L^p$ is compact for $1 \leq p < \infty$ ([9], p274), while for any compact operator $A : V \rightarrow W$ with V and W Banach spaces, $u_k \rightharpoonup u$ in V implies $Au_k \rightarrow Au$ in W ([4], Theorem 7.1-5 on p348).

2.2 Equilibrium equation and its linearized system

Constrained minimization problems can usually be reduced to unconstrained minimization problems by introducing Lagrange multipliers. We consider the following non-dimensionalized energy functional

$$\begin{aligned} \mathcal{E}(\mathbf{u}, p, \mathbf{n}, \lambda) = & \int_{\Omega} (|F|^2 - (1-a)|F^T \mathbf{n}|^2) + b|\nabla \mathbf{n}|^2 \\ & - p(\det F - 1) + \lambda(|\mathbf{n}|^2 - 1) - \int_{\Omega} \mathbf{f} \cdot \mathbf{u} - \int_{\Gamma_2} \mathbf{g} \cdot \mathbf{u} \end{aligned} \quad (23)$$

where p is the Lagrange multiplier for the incompressibility constraint $\det(I + \nabla \mathbf{u}) = 1$, which can be interpreted as ‘‘pressure’’, while λ is the Lagrange multiplier for the unity constraint $|\mathbf{n}| = 1$.

Assume $(\mathbf{u}, \mathbf{n}, p, \lambda)$ minimizes the non-dimensionalized energy (23). Then for any test function \mathbf{v} , the function $\mathcal{E}(\varepsilon) = \mathcal{E}(\mathbf{u} + \varepsilon \mathbf{v}, p, \mathbf{n}, \lambda)$ has a minimum at $\varepsilon = 0$. Thus we have

$$0 = \frac{d\mathcal{E}}{d\varepsilon}(0) \quad (24)$$

from which we can get the following equation

$$\begin{aligned} 0 = & \int_{\Omega} 2(F : \nabla \mathbf{v} - (1-a)(F^T \mathbf{n}, \nabla \mathbf{v}^T \mathbf{n})) - p \frac{\partial \det}{\partial F} : \nabla \mathbf{v} \\ & - \int_{\Omega} \mathbf{f} \cdot \mathbf{v} - \int_{\Gamma_2} \mathbf{g} \cdot \mathbf{v} da \end{aligned}$$

By similarly taking the variations $\mathbf{n} \rightarrow \mathbf{n} + \varepsilon \mathbf{m}$, $p \rightarrow p + \varepsilon q$, or $\lambda \rightarrow \lambda + \varepsilon \mu$, we get the following set of Euler-Lagrange equations

$$\begin{aligned} 0 = & \int_{\Omega} 2(F : \nabla \mathbf{v} - (1-a)(F^T \mathbf{n}, \nabla \mathbf{v}^T \mathbf{n})) - p \frac{\partial \det}{\partial F} : \nabla \mathbf{v} \\ & - \int_{\Omega} \mathbf{f} \cdot \mathbf{v} - \int_{\Gamma_2} \mathbf{g} \cdot \mathbf{v} da \\ 0 = & \int_{\Omega} -2(1-a)(F^T \mathbf{n}, F^T \mathbf{m}) + 2b(\nabla \mathbf{m}, \nabla \mathbf{n}) + 2\lambda(\mathbf{n}, \mathbf{m}) \\ 0 = & \int_{\Omega} -q(\det F - 1) \\ 0 = & \int_{\Omega} \mu((\mathbf{n}, \mathbf{n}) - 1) \end{aligned}$$

in which we seek solutions $(\mathbf{u}, \mathbf{n}, p, \lambda) \in \mathbf{H}_{\mathbf{g}|_{\Gamma_0}}^1 \times \mathbf{H}_{\mathbf{g}'|_{\Gamma_1}}^1 \times L^2(\Omega) \times L^2(\Omega)$. Correspondingly, the test functions $(\mathbf{v}, \mathbf{m}, q, \mu)$ are in $\mathbf{H}_{0|\Gamma_0}^1 \times \mathbf{H}_{0|\Gamma_1}^1 \times L^2(\Omega) \times L^2(\Omega)$. Here $H_{\mathbf{g}|_{\Gamma_0}}^1$ is defined as

$$H_{\mathbf{g}|_{\Gamma_0}}^1 = \{v \in H^1(\Omega; \mathbb{R}), v|_{\Gamma_0} = \mathbf{g}\}$$

and $\mathbf{H}_{\mathbf{g}|_{\Gamma_0}}^1$ is the corresponding vector version.

We linearize the Euler-Lagrange equation around a solution $(\mathbf{u}, \mathbf{n}, p, \lambda)$, and get the following linearized equations:

$$a_1(\mathbf{w}, \mathbf{v}) + a_2(\mathbf{l}, \mathbf{v}) + b_1(o, \mathbf{v}) = L_1(\mathbf{v}) \quad \forall \mathbf{v} \in \mathbb{V} \quad (25)$$

$$a_2(\mathbf{m}, \mathbf{w}) + a_3(\mathbf{l}, \mathbf{m}) + b_2(\gamma, \mathbf{m}) = L_2(\mathbf{m}) \quad \forall \mathbf{m} \in \mathbb{M} \quad (26)$$

$$b_1(q, \mathbf{w}) = L_3(q) \quad \forall q \in \mathbb{P} \quad (27)$$

$$b_2(\mu, \mathbf{l}) = L_4(\mu) \quad \forall \mu \in \Lambda \quad (28)$$

where $\mathbb{V} = \mathbf{H}_{0|\Gamma_0}^1$, $\mathbb{M} = \mathbf{H}_{0|\Gamma_1}^1$, $\mathbb{P} = L^2(\Omega)$, $\Lambda = H_{\Gamma_1}^{-1}$, and $(\mathbf{w}, \mathbf{l}, o, \gamma) \in \mathbb{V} \times \mathbb{M} \times \mathbb{P} \times \Lambda$ is the change in the solution, $(\mathbf{v}, \mathbf{m}, q, \mu) \in \mathbb{V} \times \mathbb{M} \times \mathbb{P} \times \Lambda$ is a test function. Here $H_{\Gamma_1}^{-1}$ is the dual space of $H_{0|\Gamma_1}^1$. We'll abuse the notation and use $\|\cdot\|_{-1}$ to also denote the norm in the $H_{\Gamma_1}^{-1}$ space. The bilinear forms in the linearized system are defined in the following equations

$$a_1(\mathbf{w}, \mathbf{v}) = \int_{\Omega} 2(\nabla \mathbf{w}, \nabla \mathbf{v}) - 2(1-a)(\nabla \mathbf{w}^T \mathbf{n}, \nabla \mathbf{v}^T \mathbf{n}) - p \left(\frac{\partial^2 \det}{\partial F^2} \nabla \mathbf{w} \right) : \nabla \mathbf{v} \quad (29)$$

$$a_2(\mathbf{m}, \mathbf{v}) = \int_{\Omega} -2(1-a)(F^T \mathbf{m}, \nabla \mathbf{v}^T \mathbf{n}) - 2(1-a)(F^T \mathbf{n}, \nabla \mathbf{v}^T \mathbf{m}) \quad (30)$$

$$a_3(\mathbf{l}, \mathbf{m}) = \int_{\Omega} -2(1-a)(F^T \mathbf{l}, F^T \mathbf{m}) + 2b(\nabla \mathbf{m}, \nabla \mathbf{l}) + 2\lambda(\mathbf{l}, \mathbf{m}) \quad (31)$$

$$b_1(q, \mathbf{w}) = \int_{\Omega} -q \frac{\partial \det}{\partial F} : \nabla \mathbf{w} \quad (32)$$

$$b_2(\mu, \mathbf{l}) = \int_{\Omega} 2\mu(\mathbf{l}, \mathbf{n}) \quad (33)$$

2.3 The stress-free state

From the Euler-Lagrange equations, we can get the following strong form partial differential equations:

$$-\operatorname{div} \sigma = \mathbf{f} \quad \text{in } \Omega \quad (34)$$

$$b \operatorname{div}(\nabla \mathbf{n}) + (1-a) \mathbf{n}^T F F^T - \lambda \mathbf{n}^T = 0 \quad \text{in } \Omega \quad (35)$$

$$\det F = 1 \quad \text{in } \Omega \quad (36)$$

$$(\mathbf{n}, \mathbf{n}) = 1 \quad \text{in } \Omega \quad (37)$$

and the following natural boundary conditions:

$$\begin{aligned} \sigma \vec{\nu} &= \mathbf{g} & \text{on } \partial\Omega \setminus \Gamma_0 \\ \nabla \mathbf{n} \vec{\nu} &= 0 & \text{on } \partial\Omega \setminus \Gamma_1 \end{aligned}$$

where the Piola-Kirchhoff stress tensor is

$$\sigma = 2 \left(I - (1-a) \mathbf{n} \mathbf{n}^T \right) F - p \frac{\partial \det}{\partial F} \quad (38)$$

Notice that if we choose the displacement to be $\mathbf{u} \equiv 0$ and the director to be $\mathbf{n} \equiv (0, 1)^T$, then we have

$$\sigma = \begin{pmatrix} 2-p & 0 \\ 0 & 2a-p \end{pmatrix}$$

If there is zero body force, equation (34) implies that p must be a constant. Then there is no way to make this σ zero if $a \neq 1$. However, it can be verified that the stress-free state can be achieved with

$$F = \begin{pmatrix} a^{1/4} & 0 \\ 0 & a^{-1/4} \end{pmatrix} \quad (39)$$

and

$$\begin{aligned} \mathbf{n} &\equiv (0, 1)^T \\ p &= 2\sqrt{a} \\ \lambda &= (1-a)/\sqrt{a} \end{aligned}$$

Remark The above observation implies that the reference configuration (strain-free state) for the BTW model is different from the stress-free configuration. It can be verified that if we take the reference state to be the stress-free state instead, then the BTW model becomes the so-called “general BTW” model

$$W_{BTW} = \frac{1}{2} \mu \text{tr}(L_0 F^T L^{-1} F) \quad (40)$$

where

$$L(\mathbf{n}) = a^{-1/2} \mathbf{n} \mathbf{n}^T + a^{1/2} (I - \mathbf{n} \mathbf{n}^T)$$

is the so-called *step tensor*, and $L_0 = L(\mathbf{n}_0)$ is the step tensor at the stress-free state.

2.4 Well-posedness of the linearized system

By adding (25) and (26) together, and adding (27)-(28) together, we can reduce the linearized system into a standard saddle point system

$$a(\tilde{\mathbf{w}}, \tilde{\mathbf{v}}) + b(\tilde{\sigma}, \tilde{\mathbf{v}}) = \tilde{L}_1(\tilde{\mathbf{v}}) \quad \forall \tilde{\mathbf{v}} \in \tilde{\mathbb{V}} \quad (41)$$

$$b(\tilde{q}, \tilde{\mathbf{w}}) = \tilde{L}_2(\tilde{q}) \quad \forall \tilde{q} \in \tilde{\mathbb{P}} \quad (42)$$

where $\tilde{\mathbb{V}} = \mathbb{V} \times \mathbb{M}$, $\tilde{\mathbb{P}} = \mathbb{P} \times \Lambda$, and

$$a(\tilde{\mathbf{w}}, \tilde{\mathbf{v}}) = a_1(\mathbf{w}, \mathbf{v}) + a_2(\mathbf{l}, \mathbf{v}) + a_2(\mathbf{m}, \mathbf{v}) + a_3(\mathbf{l}, \mathbf{m}) \quad (43)$$

$$b(\tilde{q}, \tilde{\mathbf{v}}) = b_1(q, \mathbf{v}) + b_2(\mu, \mathbf{m}) \quad (44)$$

The well-posedness of saddle point systems are well established. Here we quote the so-called Ladyzenskaya-Babuska-Brezzi theorem from [18].

Theorem 8 (Ladyzenskaya-Babuska-Brezzi). *Consider the following saddle point problem*

$$a(u, v) + b(p, v) = L_V(v) \quad \forall v \in \mathbb{V}, u \in \mathbb{V} \quad (45)$$

$$b(q, u) = L_P(q) \quad \forall q \in \mathbb{P}, p \in \mathbb{P} \quad (46)$$

with \mathbb{V} and \mathbb{P} given Hilbert spaces, L_V and L_P belonging to \mathbb{V}' and \mathbb{P}' respectively. Moreover, a and b are continuous bilinear forms defined on $\mathbb{V} \times \mathbb{V}$ and $\mathbb{P} \times \mathbb{V}$, respectively. Define the operators

$$\mathcal{B} : \mathbb{V} \rightarrow \mathbb{P}'$$

$$v \mapsto \mathcal{B}v \text{ such that } \langle \mathcal{B}v, q \rangle = b(q, v) \quad \forall q \in \mathbb{P}$$

$$\mathcal{A} : \text{Ker} \mathcal{B} \rightarrow (\text{Ker} \mathcal{B})'$$

$$w \mapsto \mathcal{A}w \text{ such that } \langle \mathcal{A}w, v \rangle = a(w, v) \quad \forall v \in \text{Ker} \mathcal{B}$$

Then the operator \mathcal{B} is onto if and only if the spaces \mathbb{V} and \mathbb{P} satisfy the following inf-sup condition:

$$\inf_{q \in \mathbb{P}, \|q\|=1} \sup_{v \in \mathbb{V}, \|v\|=1} b(q, v) \geq \beta > 0 \quad (47)$$

Moreover, the mixed problem is well-posed if and only if \mathcal{B} is onto and \mathcal{A} is invertible.

Remark The operator \mathcal{A} is invertible if and only if the following inf-sup condition is satisfied

$$\inf_{w \in \text{Ker} \mathcal{B}} \sup_{v \in \text{Ker} \mathcal{B}} \frac{a(w, v)}{\|w\| \|v\|} \geq \alpha > 0 \quad (48)$$

For some mixed system, we can prove the so called “ellipticity” condition

$$\inf_{v \in \text{Ker} \mathcal{B}} \frac{a(v, v)}{\|v\|^2} \geq \alpha > 0, \quad (49)$$

which is a stronger condition than the inf-sup condition (48). Thus the ellipticity condition (49) together with (47), will give us a sufficient condition for the well-posedness of the saddle point system (45)-(46).

Theorem 9. *The inf-sup condition for $b(\tilde{q}, \tilde{\mathbf{v}}) = b_1(q, \mathbf{v}) + b_2(\mu, \mathbf{m})$ is satisfied if and only if the corresponding inf-sup conditions for $b_1(q, \mathbf{v})$ and $b_2(\mu, \mathbf{m})$ are satisfied.*

Proof. First if the inf-sup condition for $b(\tilde{q}, \tilde{\mathbf{v}})$ is satisfied, then by Theorem 8, we know that the operator

$$\begin{aligned} \mathcal{B} : \mathbb{V} \times \mathbb{M} &\rightarrow \mathbb{P}' \times \Lambda' \\ (\mathbf{v}, \mathbf{m}) &\mapsto \mathcal{B}(\mathbf{v}, \mathbf{m}) \text{ such that } \langle \mathcal{B}(\mathbf{v}, \mathbf{m}), (q, \mu) \rangle = b_1(q, \mathbf{v}) + b_2(\mu, \mathbf{m}) \quad \forall (q, \mu) \in \mathbb{P} \times \Lambda \end{aligned}$$

is onto. Therefore, the operator

$$\begin{aligned} \mathcal{B}_1 : \mathbb{V} &\rightarrow \mathbb{P}' \\ \mathbf{v} &\mapsto \mathcal{B}_1 \mathbf{v} \text{ such that } \langle \mathcal{B}_1 \mathbf{v}, q \rangle = b_1(q, \mathbf{v}) \quad \forall q \in \mathbb{P} \end{aligned}$$

and the operator

$$\begin{aligned} \mathcal{B}_2 : \mathbb{M} &\rightarrow \Lambda' \\ \mathbf{m} &\mapsto \mathcal{B}_2 \mathbf{m} \text{ such that } \langle \mathcal{B}_2 \mathbf{m}, \mu \rangle = b_2(\mu, \mathbf{m}) \quad \forall \mu \in \Lambda \end{aligned}$$

are both onto. Thus by Theorem 8, the inf-sup conditions for $b_1(q, \mathbf{v})$ and $b_2(\mu, \mathbf{m})$ are satisfied.

Conversely, if the inf-sup conditions $b_1(q, \mathbf{v})$ and $b_2(\mu, \mathbf{m})$ are satisfied, then the operators \mathcal{B}_1 and \mathcal{B}_2 are both onto. Thus the operator \mathcal{B} is also onto. Therefore we have the inf-sup condition for $b(\tilde{q}, \tilde{\mathbf{v}}) = b_1(q, \mathbf{v}) + b_2(\mu, \mathbf{m})$. \square

Therefore, to verify the inf-sup condition for $b(\tilde{q}, \tilde{\mathbf{v}}) = b_1(q, \mathbf{v}) + b_2(\mu, \mathbf{m})$, it's enough to verify the inf-sup conditions for $b_1(q, \mathbf{v})$ and $b_2(\mu, \mathbf{m})$ individually. Notice that the bilinear form $b_1(q, \mathbf{v})$ in (32) is exactly the one in the incompressible elasticity [18], while $b_2(\mu, \mathbf{m})$ in (33) is exactly the one in the harmonic map problem [12].

For the inf-sup condition for $b_1(q, \mathbf{v})$, it's well-known that it's satisfied at the strain-free state, where $F = I$, and the inf-sup condition is reduced to the one in the Stokes problem:

$$\inf_{q \in L^2(\Omega)} \sup_{\mathbf{v} \in \mathbf{H}_{0|\Gamma_0}^1(\Omega)} \frac{\langle q, \operatorname{div}(\mathbf{v}) \rangle}{\|q\|_0 \|\mathbf{v}\|_1} \geq \beta_1 > 0 \quad (50)$$

Since the stress-free state has constant F matrix, by change of variables, it's easy to verify that the inf-sup condition for $b_1(q, \mathbf{v})$ is satisfied at the *stress-free* state, as well. In the general case that $\mathbf{u} \neq 0$ and F is not a constant, analytical verification of the inf-sup condition for $b_1(q, \mathbf{v})$ can be very difficult.

As for the inf-sup condition for $b_2(\mu, \mathbf{m})$, a slight modification of the proof in [12] gives us the following theorem:

Theorem 10. *Assume $\mathbf{n} \in \mathbf{H}_{\mathbf{n}_0|\Gamma_1}^1(\Omega) \cap W^{1,\infty}(\Omega)$, then the second inf-sup condition for $b_2(\mu, \mathbf{m})$ is satisfied, that is*

$$\inf_{\mu \in H_{\Gamma_1}^{-1}(\Omega)} \sup_{\mathbf{m} \in \mathbf{H}_{0|\Gamma_1}^1(\Omega)} \frac{\langle 2\mathbf{n} \cdot \mathbf{m}, \mu \rangle}{\|\mathbf{m}\|_1 \|\mu\|_{-1}} \geq \beta_2 > 0. \quad (51)$$

Finally, for the ellipticity condition for the bilinear form $a(\tilde{\mathbf{w}}, \tilde{\mathbf{v}})$, it's generally very complicated to verify due to the complexity of the expressions of $a_1(\cdot, \cdot)$, $a_2(\cdot, \cdot)$ and $a_3(\cdot, \cdot)$. However, it can be verified that at the stress-free state, the ellipticity condition for $a(\tilde{\mathbf{w}}, \tilde{\mathbf{v}})$ is *not* satisfied. This doesn't necessarily mean that the linearized system (25)-(28) is not well-posed, though. After all, as remarked before, the ellipticity condition is a sufficient condition, not a necessary condition.

3 Discretization

In the elastomer problem, we have the following variables to solve:

- The displacement vector field \mathbf{u} and the pressure p , which is also the Lagrange multiplier for the incompressibility constraint $\det(F) - 1 = 0$,
- The director vector field \mathbf{n} and the Lagrange multiplier λ for the unity constraint $|\mathbf{n}|^2 - 1 = 0$.

The first pair (\mathbf{u}, p) is similar to those in the incompressible elasticity, and we'll use the Taylor-Hood element $P_2 - P_1$ for (\mathbf{u}, p) . That is continuous piecewise quadratic finite element for \mathbf{u} , and continuous piecewise linear finite element for p . The Taylor-Hood element has been proved ([18]) to be stable at least at the strain-free state $\mathbf{u} = 0$. The second pair (\mathbf{n}, λ) is similar to those in the harmonic map problem, and we will use piecewise linear finite element for both \mathbf{n} and λ , as Winther et al. did in [12]. Notice that it's crucial to impose Dirichlet boundary conditions for \mathbf{n} and λ at the same boundary to make sure that $|\mathbf{n}| = 1$ is satisfied at all the mesh nodes.

Let V_h denote the space of continuous piecewise linear functions and $V_{h,g|\Gamma_0} = \{v \in V_h \cap H^1 : v = g \text{ on } \Gamma_0\}$. Let \mathbf{V}_h and $\mathbf{V}_{h,g|\Gamma_0}$ be the corresponding vector version. Let π_h be the nodal interpolation operators onto the spaces V_h and \mathbf{V}_h .

Let W_h denote the space of continuous piecewise quadratic functions and $W_{h,g|\Gamma_0} = \{w \in W_h \cap H^1 : w = g \text{ on } \Gamma_0\}$. Let \mathbf{W}_h and $\mathbf{W}_{h,g|\Gamma_0}$ be the corresponding vector version.

3.1 Existence of the discrete minimization problem

Let

$$K_h = \{\mathbf{u}_h \in \mathbf{W}_{h,0|\Gamma_0} + \mathbf{u}_{0h}, \int_{\Omega} q_h(\det(I + \nabla \mathbf{u}_h) - 1)dx = 0, \forall q_h \in V_h\} \quad (52)$$

$$N_h = \{\mathbf{n}_h \in \mathbf{V}_{h,0|\Gamma_1} + \mathbf{n}_{0h}, \int_{\Omega} \mu_h \pi_h(|\mathbf{n}_h|^2 - 1)dx = 0, \forall \mu_h \in V_{h,0|\Gamma_1}\} \quad (53)$$

Define the admissible set

$$\mathcal{A}(\mathbf{u}_{0h}, \mathbf{n}_{0h}) = K_h \times N_h \quad (54)$$

Notice that $\mathbf{n}_h \in N_h$ if and only if the function $\pi_h(|\mathbf{n}_h|^2 - 1) \in V_{h,0|\Gamma_1}$ is identically 0, which means $|\mathbf{n}_h| = 1$ at all the mesh nodes.

Let $\varphi_j, j = 1, \dots, N$ be a basis of V_h , and $\psi_j, j = 1, \dots, M$ be a basis of $V_{h,0|\Gamma_1}$. And define

$$g_j(\mathbf{u}_h, \mathbf{n}_h) = \begin{cases} \int_{\Omega} \varphi_j(\det(I + \nabla \mathbf{u}_h) - 1)dx & 1 \leq j \leq N \\ \int_{\Omega} \psi_{j-N} \pi_h(|\mathbf{n}_h|^2 - 1)dx & N + 1 \leq j \leq N + M \end{cases} \quad (55)$$

Then g_j is a continuous function on $(\mathbf{W}_{h,0|\Gamma_0} + \mathbf{u}_{0h}) \times (\mathbf{V}_{h,0|\Gamma_1} + \mathbf{n}_{0h})$. Therefore $\mathcal{A}(\mathbf{u}_{0h}, \mathbf{n}_{0h})$ can be written as the intersection of reciprocal images of 0 of the continuous functions g_j . Thus it's closed in $(\mathbf{W}_{h,0|\Gamma_0} + \mathbf{u}_{0h}) \times (\mathbf{V}_{h,0|\Gamma_1} + \mathbf{n}_{0h})$.

Define the energy functional

$$\begin{aligned} \Pi(\mathbf{u}, \mathbf{n}) &= \int_{\Omega} (|F|^2 - (1-a)|F^T \mathbf{n}|^2) + b|\nabla \mathbf{n}|^2 \\ &\quad - \int_{\Omega} \mathbf{f} \cdot \mathbf{u} - \int_{\Gamma_2} \mathbf{g} \cdot \mathbf{u} da \end{aligned} \quad (56)$$

where $F = I + \nabla \mathbf{u}$. Then the discrete formulation of the minimization problem is

$$\text{Find } (\mathbf{u}_h, \mathbf{n}_h) \in \mathcal{A}(\mathbf{u}_{0h}, \mathbf{n}_{0h}), \text{ minimizing } \Pi \text{ on } \mathcal{A}(\mathbf{u}_{0h}, \mathbf{n}_{0h}). \quad (57)$$

Lemma 11. Assume $\mathbf{n} \in N_h$ and $0 \leq a \leq 1$, then for any matrix $F \in \mathbb{M}^{2 \times 2}$, we have

$$(|F|^2 - (1-a)|F^T \mathbf{n}|^2) \geq a|F|^2 \quad (58)$$

Proof. Take any point $x \in \Omega$, suppose it's in the triangle $\triangle P_1 P_2 P_3$. Since $\mathbf{n} \in N_h$, we have

$$\mathbf{n}(x) = \lambda_1 \mathbf{n}(P_1) + \lambda_2 \mathbf{n}(P_2) + \lambda_3 \mathbf{n}(P_3)$$

where $\lambda_i, i = 1, 2, 3$ are barycentric coordinates. As pointed out above, $\mathbf{n} \in N_h$ if and only if $|\mathbf{n}| = 1$ at all the mesh nodes. Thus we have

$$\begin{aligned} |\mathbf{n}(x)| &= |\lambda_1 \mathbf{n}(P_1) + \lambda_2 \mathbf{n}(P_2) + \lambda_3 \mathbf{n}(P_3)| \\ &\leq \lambda_1 |\mathbf{n}(P_1)| + \lambda_2 |\mathbf{n}(P_2)| + \lambda_3 |\mathbf{n}(P_3)| \\ &= \lambda_1 + \lambda_2 + \lambda_3 \\ &= 1 \end{aligned}$$

If $|\mathbf{n}(x)| = 0$, then obviously the conclusion is true. In the following, we assume $|\mathbf{n}(x)| > 0$.

Let $\hat{\mathbf{n}} = \mathbf{n}(x)/|\mathbf{n}(x)|$, then $|\hat{\mathbf{n}}| = 1$. We have

$$\begin{aligned} &(|F|^2 - (1-a)|F^T \mathbf{n}|^2) \\ &= (|F|^2 - (1-a)|\mathbf{n}(x)|^2 |F^T \hat{\mathbf{n}}|^2) \\ &\geq (|F|^2 - (1-a)|F^T \hat{\mathbf{n}}|^2) \\ &\geq a|F|^2 \end{aligned}$$

where in the last step we have used Proposition 4. □

Remark Similar arguments work for 3D, as well.

Theorem 12. *There exists solution to the discrete minimization problem (57).*

Proof. Take any $(\mathbf{u}_h, \mathbf{n}_h) \in \mathcal{A}(\mathbf{u}_{0h}, \mathbf{n}_{0h})$, we have by Lemma 11

$$\begin{aligned} \Pi(\mathbf{u}_h, \mathbf{n}_h) &\geq \int_{\Omega} a|(I + \nabla \mathbf{u}_h)|^2 + b|\nabla \mathbf{n}_h|^2 dx \\ &\quad - \|\mathbf{f}\|_{L^2(\Omega)} \|\mathbf{u}_h\|_{L^2(\Omega)} - \|\mathbf{g}\|_{L^2(\Gamma_2)} \|\mathbf{u}_h\|_{L^2(\Gamma_2)} \\ &\geq \int_{\Omega} a|(I + \nabla \mathbf{u}_h)|^2 + b|\nabla \mathbf{n}_h|^2 dx \\ &\quad - \left(\frac{1}{\varepsilon} \|\mathbf{f}\|_{L^2(\Omega)}^2 + \varepsilon \|\mathbf{u}_h\|_{L^2(\Omega)}^2 \right) - \left(\frac{1}{\varepsilon} \|\mathbf{g}\|_{L^2(\Gamma_2)}^2 + \varepsilon \|\mathbf{u}_h\|_{L^2(\Gamma_2)}^2 \right) \\ &\geq \int_{\Omega} C_1 |(I + \nabla \mathbf{u}_h)|^2 + C_2 |\nabla \mathbf{n}_h|^2 dx - C_3 \end{aligned}$$

where $\varepsilon > 0$ is small and $C_i > 0, i = 1, 2, 3$ are constants and we have applied the generalized Poincaré inequality ([4], p281) and the Trace Theorem ([9], p258) in the last step. Thus $\Pi(\mathbf{u}_h, \mathbf{n}_h) \rightarrow \infty$ as $\|\mathbf{u}_h\|_1$ or $\|\mathbf{n}_h\|_1$ goes to ∞ . Therefore its minimum must be achieved at a bounded subset of $\mathcal{A}(\mathbf{u}_{0h}, \mathbf{n}_{0h})$.

On the other hand, since \mathcal{A} is the intersection of reciprocal images of 0 of the continuous functions g_j , it's a closed set.

Now we are minimizing a continuous function $\Pi(\mathbf{u}_h, \mathbf{n}_h)$ on a closed bounded *finite-dimensional* set, by the Weierstrass Theorem, we can find $(\mathbf{u}_h, \mathbf{n}_h) \in \mathcal{A}(\mathbf{u}_{0h}, \mathbf{n}_{0h})$ minimizing Π on $\mathcal{A}(\mathbf{u}_{0h}, \mathbf{n}_{0h})$. □

Remark This theorem is the discrete version of Theorem 7. Since we are dealing with finite dimensional spaces, the proof is much simpler. Plus, in the continuous case we were only able to prove Theorem 7 for 2D, but in the discrete case, it's easy to see that the proof above applies to 3D, too.

3.2 Equilibrium equation and its linearization

Similar to the continuous case, we start with the following energy functional with Lagrange multipliers

$$\begin{aligned} \mathcal{E}(\mathbf{u}_h, \mathbf{n}_h, p_h, \lambda_h) &= \int_{\Omega} (|F_h|^2 - (1-a)|F_h^T \mathbf{n}_h|^2) + b|\nabla \mathbf{n}_h|^2 \\ &\quad - p_h(\det(F_h) - 1) + \lambda(\pi_h(\mathbf{n}_h, \mathbf{n}_h) - 1) \\ &\quad - \int_{\Omega} \mathbf{f} \cdot \mathbf{u}_h - \int_{\Gamma_2} \mathbf{g} \cdot \mathbf{u}_h da \end{aligned} \quad (59)$$

where $F_h = I + \nabla \mathbf{u}_h$ is the deformation gradient.

Taking the first variation variation on (59) gives us the Euler-Lagrange equations (equilibrium equations) for the constrained minimization problem (57), and taking another variation on the Euler-Lagrange equations gives us the linearized problems.

Thus the equilibrium equations are, find $(\mathbf{u}_h, \mathbf{n}_h, p_h, \lambda_h) \in \mathbf{W}_{h, \mathbf{u}_0|_{\Gamma_0}} \times \mathbf{V}_{h, \mathbf{n}_0|_{\Gamma_1}} \times V_h \times V_{h, \lambda_0|_{\Gamma_1}}$, such that

$$\begin{aligned} 0 &= \int_{\Omega} 2(F_h : \nabla \mathbf{v} - (1-a)(F_h^T \mathbf{n}_h, \nabla \mathbf{v}^T \mathbf{n}_h)) - p_h \frac{\partial \det}{\partial F_h} : \nabla \mathbf{v} \\ &\quad - \int_{\Omega} \mathbf{f} \cdot \mathbf{v} - \int_{\Gamma_2} \mathbf{g} \cdot \mathbf{v} da \end{aligned} \quad (60)$$

$$0 = \int_{\Omega} -2(1-a)(F_h^T \mathbf{n}_h, F_h^T \mathbf{m}) + 2b(\nabla \mathbf{m}, \nabla \mathbf{n}_h) + 2\lambda_h \pi_h(\mathbf{n}_h, \mathbf{m}) \quad (61)$$

$$0 = \int_{\Omega} -q(\det F_h - 1) \quad (62)$$

$$0 = \int_{\Omega} \mu \pi_h((\mathbf{n}_h, \mathbf{n}_h) - 1) \quad (63)$$

for any test functions $(\mathbf{v}, \mathbf{m}, q, \mu) \in \mathbf{W}_{h,0|_{\Gamma_0}} \times \mathbf{V}_{h,0|_{\Gamma_1}} \times V_h \times V_{h,0|_{\Gamma_1}}$, where $F_h = I + \nabla \mathbf{u}_h$.

The corresponding linearized problem is, for a given $(\mathbf{u}_h, \mathbf{n}_h, p_h, \lambda_h) \in \mathbf{W}_{h, \mathbf{u}_0|_{\Gamma_0}} \times \mathbf{V}_{h, \mathbf{n}_0|_{\Gamma_1}} \times V_h \times V_{h, \lambda_0|_{\Gamma_1}}$, find $(\mathbf{w}, \mathbf{l}, o, \gamma) \in \mathbf{W}_{h,0|_{\Gamma_0}} \times \mathbf{V}_{h,0|_{\Gamma_1}} \times V_h \times V_{h,0|_{\Gamma_1}}$ such that

$$a_1(\mathbf{w}, \mathbf{v}) + a_2(\mathbf{l}, \mathbf{v}) + b_1(o, \mathbf{v}) = L_1(\mathbf{v}) \quad (64)$$

$$a_2(\mathbf{m}, \mathbf{w}) + a_3(\mathbf{l}, \mathbf{m}) + b_2(\gamma, \mathbf{m}) = L_2(\mathbf{m}) \quad (65)$$

$$b_1(q, \mathbf{w}) = L_3(q) \quad (66)$$

$$b_2(\mu, \mathbf{l}) = L_4(\mu) \quad (67)$$

is true for any $(\mathbf{v}, \mathbf{m}, q, \mu) \in \mathbf{W}_{h,0|_{\Gamma_0}} \times \mathbf{V}_{h,0|_{\Gamma_1}} \times V_h \times V_{h,0|_{\Gamma_1}}$. Here a_1, a_2 and b_1 are the same as in the continuous case, while

$$a_3(\mathbf{l}, \mathbf{m}) = \int_{\Omega} -2(1-a)(F_h^T \mathbf{l}, F_h^T \mathbf{m}) + 2b(\nabla \mathbf{m}, \nabla \mathbf{l}) + 2\lambda_h \pi_h(\mathbf{l}, \mathbf{m}) \quad (68)$$

and

$$b_2(\mu, \mathbf{m}) = \int_{\Omega} 2\mu \pi_h(\mathbf{n}_h, \mathbf{m}) \quad (69)$$

3.3 Well-posedness of the linearized system

As in the continuous case, the well-posedness of the linearized system can be reduced to the verification of the inf-sup conditions for the bilinear forms $b_1(\cdot, \cdot)$, $b_2(\cdot, \cdot)$ and $a(\cdot, \cdot)$.

Since we used the Taylor-Hood element $\mathbf{P}_2 - P_1$ for the (\mathbf{u}, p) combination, the inf-sup condition for $b_1(\cdot, \cdot)$ is at least satisfied at the strain-free state (Proposition 6.1 of [3]). Since at the stress-free state the deformation gradient F is a constant, by change of variables, it's easy to verify that the inf-sup condition for $b_1(\cdot, \cdot)$ is satisfied at the stress-free state, as well.

For the inf-sup condition for $b_2(\cdot, \cdot)$, we can use the results from [12]. A slight modification of the proof in [12] gives us the following result:

Theorem 13. *Assume $\mathbf{n} \in \mathbf{H}_{\mathbf{n}_0|\Gamma_1}^1(\Omega) \cap \mathbf{W}^{1,\infty}(\Omega)$, and $\mathbf{n}_h \in \mathbf{V}_{h,\mathbf{n}_0|\Gamma_1}$ satisfies $|\mathbf{n}_h| \geq C > 0$ and $\|\mathbf{n}_h - \pi_h \mathbf{n}\|_1 \leq \gamma/|\log(h)|^{1/2}$. Then we can find a positive constant β_2 , independent of h , such that*

$$\inf_{\mu \in \mathbf{V}_{h,0|\Gamma_1}} \sup_{\mathbf{m} \in \mathbf{V}_{h,0|\Gamma_1}} \frac{\langle \pi_h[\mathbf{n}_h \cdot \mathbf{m}], \mu \rangle}{\|\mu\|_{-1} \|\mathbf{m}\|_1} \geq \beta_2 \quad (70)$$

In general, analytical verification of the inf-sup conditions may not be easy. However, in the discrete case, we can relate the inf-sup values to the singular values of certain matrices.

For the general inf-sup value β_h in

$$\beta_h = \inf_{q_h \in \mathbb{P}_h, \|q_h\|=1} \left\{ \sup_{v_h \in \mathbb{V}_h, \|v_h\|=1} b(q_h, v_h) \right\} \quad (71)$$

we have the following result ([3]).

Theorem 14. *The inf-sup value β_h in (71) is equal to the smallest singular value of the matrix $S^{-\frac{1}{2}}BT^{-\frac{1}{2}}$, where the matrices S, T, B are defined by the following equations*

$$\|q_h\|^2 = \mathbf{q}^T S \mathbf{q} \quad (72)$$

$$\|v_h\|^2 = \mathbf{v}^T T \mathbf{v} \quad (73)$$

$$b(q_h, v_h) = \mathbf{q}^T B \mathbf{v} \quad (74)$$

and \mathbf{q}, \mathbf{v} are the degrees of freedom of q_h and v_h respectively.

To verify the inf-sup condition or ellipticity condition for $a(\cdot, \cdot)$ on $\text{Ker}(\mathcal{B}_h)$, we are interested in calculating the inf-sup value $\hat{\beta}_h$ in

$$\hat{\beta}_h = \inf_{\|u_h\|=1} \sup_{\|v_h\|=1} a(u_h, v_h) \quad \text{on } \text{Ker}(\mathcal{B}_h) \subset \mathbb{V}_h \quad (75)$$

and the ellipticity constant $\hat{\alpha}_h$ in

$$\hat{\alpha}_h = \inf_{\|v_h\|=1} a(v_h, v_h) \quad \text{on } \text{Ker}(\mathcal{B}_h) \subset \mathbb{V}_h \quad (76)$$

as well.

Theorem 15. *The inf-sup value $\hat{\beta}_h$ in (75) is equal to the smallest singular value of the matrix A_1 , while the ellipticity constant $\hat{\alpha}_h$ in (76) is equal to the smallest eigenvalue of the matrix A_1 , where A_1 is the lower right $(n-m) \times (n-m)$ corner of the matrix $Q^T T^{-1/2} A T^{-1/2} Q$. Here n is the dimension of \mathbb{V}_h , m is the dimension of \mathbb{P}_h , and the matrices T, A, B are defined by the following equations*

$$\|v_h\|^2 = \mathbf{v}^T T \mathbf{v}$$

$$a(u_h, v_h) = \mathbf{u}^T A \mathbf{v}$$

$$v_h \in \text{Ker}(\mathcal{B}_h) \Leftrightarrow B \mathbf{v} = 0$$

where \mathbf{u}, \mathbf{v} are the degrees of freedom of u_h and v_h respectively. Here B is assumed to be full-rank and the matrix Q is defined by the QR decomposition of $(BT^{-1/2})^T$

$$(BT^{-1/2})^T = Q \begin{pmatrix} R \\ 0 \end{pmatrix}$$

Proof. First, let $\mathbf{x} = T^{\frac{1}{2}}\mathbf{u}$, $\mathbf{y} = T^{\frac{1}{2}}\mathbf{v}$ then we have

$$\hat{\beta}_h = \inf_{\mathbf{x} \in \text{Ker}(\tilde{B})} \sup_{\mathbf{y} \in \text{Ker}(\tilde{B})} \frac{\mathbf{x}^T \tilde{A} \mathbf{y}}{\sqrt{\mathbf{x}^T \mathbf{x}} \sqrt{\mathbf{y}^T \mathbf{y}}} \quad (77)$$

where $\tilde{B} = BT^{-1/2}$, and $\tilde{A} = T^{-1/2}AT^{-1/2}$.

Since \tilde{B} is full-rank, the matrix $R \in \mathbb{M}^{m \times m}$ in the QR decomposition

$$\tilde{B}^T = Q \begin{pmatrix} R \\ 0 \end{pmatrix} \quad (78)$$

is non-singular. Let

$$Q^T \mathbf{x} = \begin{pmatrix} \mathbf{w}_x \\ \mathbf{z}_x \end{pmatrix} \quad (79)$$

where $\mathbf{w}_x \in \mathbb{R}^m$ and $\mathbf{z}_x \in \mathbb{R}^{n-m}$. Then it's easy to verify that

$$\mathbf{x} \in \text{Ker}(\tilde{B}) \Leftrightarrow \mathbf{w}_x = 0$$

Thus there will be no constraint on \mathbf{z}_x . Therefore

$$\inf_{\mathbf{x} \in \text{Ker}(\tilde{B})} \sup_{\mathbf{y} \in \text{Ker}(\tilde{B})} \frac{\mathbf{x}^T \tilde{A} \mathbf{y}}{\sqrt{\mathbf{x}^T \mathbf{x}} \sqrt{\mathbf{y}^T \mathbf{y}}} = \inf_{\mathbf{z}_x} \sup_{\mathbf{z}_y} \frac{\mathbf{z}_x^T A_1 \mathbf{z}_y}{\sqrt{\mathbf{z}_x^T \mathbf{z}_x} \sqrt{\mathbf{z}_y^T \mathbf{z}_y}} \quad (80)$$

where A_1 is the lower right $(n-m) \times (n-m)$ corner of the matrix $Q^T \tilde{A} Q$. Thus $\hat{\beta}_h$ is the smallest singular value of the matrix A_1 .

Similar arguments reduce $\hat{\alpha}_h$ to the smallest eigenvalue of the matrix A_1 . \square

Remark The matrix B is full-rank if and only if the operator \mathcal{B}_h is onto, which is true if and only if the corresponding inf-sup condition holds.

To compute the inf-sup value for b_2 , we need to calculate the $H_{\Gamma_1}^{-1}$ norm for any function v_h in $V_{h,0|\Gamma_1}$. By the Riesz Representation Theorem, we can find $\tilde{v} \in H_{0|\Gamma_1}^1$, such that $\|v_h\|_{H_{\Gamma_1}^{-1}} = \|\tilde{v}\|_{H^1}$. The H^1 norm of \tilde{v} can be approximated by the H^1 norm of \hat{v}_h , which is the L^2 projection of $\tilde{v} \in H_{0|\Gamma_1}^1$ into $V_{h,0|\Gamma_1}$. Let $\{\varphi_i, i = 1, \dots, n\}$ be a basis of $V_{h,0|\Gamma_1}$. We want to assemble the matrix S such that

$$\|v_h\|_{H_{\Gamma_1}^{-1}} \approx \|\hat{v}_h\|_{H^1} = \mathbf{v}^T S \mathbf{v}$$

where $\mathbf{v} \in \mathbb{R}^n$ is the degree of freedom for v_h .

Theorem 16. *The matrix $S = AB^{-1}A$, where the matrices A and B satisfy*

$$\begin{aligned} \|v_h\|_{L^2} &= \mathbf{v}^T A \mathbf{v} \\ \|v_h\|_{H^1} &= \mathbf{v}^T B \mathbf{v} \end{aligned}$$

for any v_h in $V_{h,0|\Gamma_1}$, and $\mathbf{v} \in \mathbb{R}^n$ is the degree of freedom for v_h .

Proof. Let $f : H_{\Gamma_1}^{-1} \rightarrow V_{h,0|\Gamma_1}$ be the map taking v_h to \hat{v}_h , and let $\hat{\varphi}_i = f(\varphi_i)$. It's easy to see that

$$S_{ij} = \langle \hat{\varphi}_i, \hat{\varphi}_j \rangle_{H^1} \quad (81)$$

By definition of $\hat{\varphi}_i$, we have

$$\int \varphi_i \varphi_j = \int D \hat{\varphi}_i D \varphi_j + \int \hat{\varphi}_i \varphi_j \quad \forall 1 \leq i, j \leq n \quad (82)$$

Since $\hat{\varphi}_i \in V_{h,0|\Gamma_1}$, we can write

$$\hat{\varphi}_i = \sum_k G_{ik} \varphi_k$$

Substituting it into (82) gives

$$\int \varphi_i \varphi_j = \sum_k G_{ik} \left(\int D\varphi_k \cdot D\varphi_j + \int \varphi_k \varphi_j \right)$$

That is $A = GB$, or $G = AB^{-1}$. Therefore

$$\begin{aligned} S &= (\langle \hat{\varphi}_i, \hat{\varphi}_j \rangle_{H^1}) \\ &= (D\hat{\varphi}_i, D\hat{\varphi}_j) + (\hat{\varphi}_i, \hat{\varphi}_j) \\ &= \sum_{p,q} G_{ip} G_{jq} [(D\varphi_p, D\varphi_q) + (\varphi_p, \varphi_q)] \\ &= \sum_{p,q} (G_{ip} B_{pq} G_{qj}^T) \\ &= GBG^T \\ &= (AB^{-1})B(B^{-1}A) \\ &= AB^{-1}A \end{aligned}$$

□

3.4 Existence and Uniqueness of the Lagrange multipliers

Le Tallec proved in [15] that if the inf-sup condition is satisfied at \mathbf{u}_h , then there exists a *unique* p_h such that (\mathbf{u}_h, p_h) is a solution of the discrete equilibrium equations of the incompressible elasticity. In this section, we will prove similar results for our elastomer problem.

The proof uses the following result of Clarke [6] on constrained minimization problems, where $\partial g(x)$ is the generalized gradient introduced in [5].

Theorem 17. *Denote J a finite set of integers. We suppose given: E a Banach space, $g_0, g_j (j \in J)$ locally Lipschitz functions from E to \mathbb{R} , and C a closed subset of E . We consider the following problem:*

$$\begin{aligned} &\text{Minimize } g_0(x) \\ &\text{subject to } x \in C, \quad g_j(x) = 0, \quad \forall j \in J. \end{aligned} \quad (83)$$

If \bar{x} is a local solution of (83) then there exist real numbers r_0, s_j not all zero, and a point ξ in the dual space E' of E such that:

$$\xi \in r_0 \partial g_0(\bar{x}) + \sum_j s_j \partial g_j(\bar{x}), \quad -\xi \in N_c(\bar{x}), \quad (84)$$

where $N_c(\bar{x})$ is the normal cone at C in \bar{x} , ∂g_j is the generalized gradient of $g_j(x)$.

Theorem 18. *Suppose $(\mathbf{u}_h, \mathbf{n}_h) \in K_h \times N_h$, and at $(\mathbf{u}_h, \mathbf{n}_h)$, the inf-sup conditions for b_1 and b_2 are both satisfied. Then there exist a unique $p_h \in V_h$ and a unique $\lambda_h \in V_{h,\lambda_0|\Gamma_0}$ such that $(\mathbf{u}_h, \mathbf{n}_h, p_h, \lambda_h)$ is a solution of the discrete equilibrium equations (60)-(63).*

Proof. Denote

$$E = C = (\mathbf{W}_{h,0|\Gamma_0} + \mathbf{u}_{0h}) \times (\mathbf{V}_{h,0|\Gamma_1} + \mathbf{n}_{0h}) \quad (85)$$

$$g_0(x) = \Pi(\mathbf{v}_h, \mathbf{m}_h), \quad g_j(x) = g_j(\mathbf{v}_h, \mathbf{m}_h) \quad (86)$$

where the functions g_j are defined as in (55). It's easy to see that

$$N_C(\bar{x}) = N_E(\bar{x}) = (0, 0). \quad (87)$$

Notice that

$$\partial\Pi(\mathbf{u}_h, \mathbf{n}_h) \subset \{Dg_0^1 + Dg_0^2\} \quad (88)$$

where Dg_0^1 and Dg_0^2 are in $[(\mathbf{W}_{h,0|\Gamma_0} + \mathbf{u}_{0h}) \times (\mathbf{V}_{h,0|\Gamma_1} + \mathbf{n}_{0h})]^*$. We have

$$Dg_0^1(\mathbf{u}_h, \mathbf{n}_h) \cdot (\mathbf{v}_h, \mathbf{m}_h) = \begin{pmatrix} f_1(\mathbf{v}_h) \\ f_2(\mathbf{m}_h) \end{pmatrix}$$

where

$$f_1(\mathbf{v}) = \int_{\Omega} 2(F_h : \nabla \mathbf{v} - (1-a)(F_h^T \mathbf{n}_h, \nabla \mathbf{v}^T \mathbf{n}_h))$$

and

$$f_2(\mathbf{m}) = \int_{\Omega} -2(1-a)(F_h^T \mathbf{n}_h, F_h^T \mathbf{m}) + 2b(\nabla \mathbf{m}, \nabla \mathbf{n}_h)$$

Also,

$$Dg_0^2(\mathbf{u}_h, \mathbf{n}_h) \cdot (\mathbf{v}_h, \mathbf{m}_h) = \begin{pmatrix} -\int_{\Omega} \mathbf{f} \cdot \mathbf{v}_h - \int_{\Gamma_2} \mathbf{g} \cdot \mathbf{v}_h da \\ 0 \end{pmatrix}$$

We also note that $g_j(\mathbf{v}_h, \mathbf{m}_h)$ is continuously differentiable on $(\mathbf{W}_{h,0|\Gamma_0} + \mathbf{u}_{0h}) \times (\mathbf{V}_{h,0|\Gamma_1} + \mathbf{n}_{0h})$, and that

$$\partial g_j = \{Dg_j\}, \quad (89)$$

$$Dg_j(\mathbf{u}_h, \mathbf{n}_h) \cdot (\mathbf{v}_h, \mathbf{m}_h) = \begin{pmatrix} \int_{\Omega} -\varphi_j \frac{\partial \det}{\partial F}(I + \nabla \mathbf{u}_h) : \nabla \mathbf{v}_h \\ 0 \end{pmatrix}$$

for $1 \leq j \leq N$ (90)

$$Dg_j(\mathbf{u}_h, \mathbf{n}_h) \cdot (\mathbf{v}_h, \mathbf{m}_h) = \begin{pmatrix} 0 \\ \int_{\Omega} \psi_{j-N} \pi_h [2\mathbf{n}_h \cdot \mathbf{m}_h] dx \end{pmatrix}$$

for $N+1 \leq j \leq N+M$ (91)

Therefore applying Theorem 17, we have:

There exists real numbers r_0, s_j not all zero, such that

$$0 \in r_0 \partial\Pi(\mathbf{u}_h, \mathbf{n}_h) + \sum_{j=1}^{N+M} s_j \partial g_j(\mathbf{u}_h, \mathbf{n}_h) \quad (92)$$

Using (88) and (89), equation (92) becomes

$$r_0 \{Dg_0^1(\mathbf{u}_h, \mathbf{n}_h) + Dg_0^2(\mathbf{u}_h, \mathbf{n}_h)\} + \sum_{j=1}^{N+M} s_j Dg_j(\mathbf{u}_h, \mathbf{n}_h) = 0$$

in $[(\mathbf{W}_{h,0|\Gamma_0} + \mathbf{u}_{0h}) \times (\mathbf{V}_{h,0|\Gamma_1} + \mathbf{n}_{0h})]^*$. (93)

Suppose now $r_0 = 0$. By linearity, and using equations (90), (91), we can then transform (93) to get

$$\int_{\Omega} \left(\sum_{j=1}^N s_j \varphi_j \right) \frac{\partial \det}{\partial F}(I + \nabla \mathbf{u}_h) : \nabla \mathbf{v}_h dx = 0, \quad \forall \mathbf{v}_h \in \mathbf{W}_{h,0|\Gamma_0} \quad (94)$$

$$\int_{\Omega} \left(\sum_{j=1}^M s_{N+j} \psi_j \right) \pi_h [2\mathbf{n}_h \cdot \mathbf{m}_h] dx = 0, \quad \forall \mathbf{m}_h \in \mathbf{V}_{h,0|\Gamma_1}, \quad (95)$$

Since at least one s_j is nonzero, at least one of the equations (94) or (95) is in contradiction with the inf-sup conditions. Thus r_0 cannot be zero. We can then divide (93) by r_0 to get

$$Dg_0^1(\mathbf{u}_h, \mathbf{n}_h) \cdot (\mathbf{v}_h, \mathbf{m}_h) + 1/r_0 \sum_{j=1}^M s_j Dg_j(\mathbf{u}_h, \mathbf{n}_h) = -Dg_0^2(\mathbf{u}_h, \mathbf{n}_h) \cdot (\mathbf{v}_h, \mathbf{m}_h),$$

$$\forall (\mathbf{v}_h, \mathbf{m}_h) \in [(\mathbf{W}_{h,0|\Gamma_0} + \mathbf{u}_{0h}) \times (\mathbf{V}_{h,0|\Gamma_1} + \mathbf{n}_{0h})] \quad (96)$$

That is

$$f_1(\mathbf{v}_h) - \int_{\Omega} p_h \frac{\partial \det}{\partial F}(I + \nabla \mathbf{u}_h) : \nabla \mathbf{v}_h dx = \int_{\Omega} \mathbf{f} \cdot \mathbf{v}_h + \int_{\Gamma_2} \mathbf{g} \cdot \mathbf{v}_h da \quad (97)$$

$$f_2(\mathbf{m}_h) + \int_{\Omega} \lambda_h \pi_h [2\mathbf{n}_h \cdot \mathbf{m}_h] dx = 0 \quad (98)$$

where we have denoted

$$p_h = \left(\sum_{j=1}^N s_j \varphi_j \right) / r_0 \quad (99)$$

$$\lambda_h = \left(\sum_{j=1}^M s_{N+j} \psi_j \right) / r_0 \quad (100)$$

Equations (97) and (98) are precisely (60)-(61). Since we also have $(\mathbf{u}_h, \mathbf{n}_h) \in K_h \times N_h$, we conclude that $(\mathbf{u}_h, \mathbf{n}_h, p_h, \lambda_h)$ is a solution of (60)-(63).

Finally, if there were two different p_h , their difference would violate the inf-sup condition for b_1 ; and if there were two different λ_h , their difference would violate the inf-sup condition for b_2 . So we have the uniqueness of both p_h and λ_h . \square

3.5 Implementation using FEniCS

All the computations in this project were done using FEniCS ([10]), which is an open source software for automated solution of differential equations.

We want to solve the equilibrium equations (60)-(63). Assume $(\bar{\mathbf{u}}, \bar{\mathbf{n}}, \bar{p}, \bar{\lambda})$ are the degrees of freedom for $(\mathbf{u}_h, \mathbf{n}_h, p_h, \lambda_h)$. Replacing the test functions $(\mathbf{v}, \mathbf{m}, q, \mu)$ by the corresponding basis functions, the equilibrium equations (60)-(63) can be looked as a nonlinear equation for $(\bar{\mathbf{u}}, \bar{\mathbf{n}}, \bar{p}, \bar{\lambda})$:

$$\mathcal{F}(\bar{\mathbf{u}}, \bar{\mathbf{n}}, \bar{p}, \bar{\lambda}) = 0 \quad (101)$$

Since it's nonlinear, we can use Newton's method to solve. The iterations are, for integers $k \geq 0$,

$$\frac{D\mathcal{F}(\bar{\mathbf{u}}^k, \bar{\mathbf{n}}^k, \bar{p}^k, \bar{\lambda}^k)}{D(\bar{\mathbf{u}}, \bar{\mathbf{n}}, \bar{p}, \bar{\lambda})}(\Delta \bar{\mathbf{u}}^k, \Delta \bar{\mathbf{n}}^k, \Delta \bar{p}^k, \Delta \bar{\lambda}^k) = -\mathcal{F}(\bar{\mathbf{u}}^k, \bar{\mathbf{n}}^k, \bar{p}^k, \bar{\lambda}^k) \quad (102)$$

It can be verified that the matrix

$$A = \frac{D\mathcal{F}(\bar{\mathbf{u}}^k, \bar{\mathbf{n}}^k, \bar{p}^k, \bar{\lambda}^k)}{D(\bar{\mathbf{u}}, \bar{\mathbf{n}}, \bar{p}, \bar{\lambda})} \quad (103)$$

is exactly the matrix corresponding to the left side of the linearized system (64)-(67) (i.e., by replacing $(\mathbf{w}, \mathbf{l}, o, \gamma)$ and $(\mathbf{v}, \mathbf{m}, q, \mu)$ by the corresponding basis functions, and replacing $(\mathbf{u}_h, \mathbf{n}_h, p_h, \lambda_h)$ by the solution at step k). Each step of (102) corresponds to a linear variational problem, and can be solved by FEniCS. Thus the whole problem can be solved.

There is a minor issue, though, about the procedure above. In both the equilibrium equations (60)-(63) and the linearized equations (64)-(67), there are terms with the interpolation operator π_h , which is *not* supported in the FEniCS form language. Thus we can't directly input those bilinear and linear forms in the form file for FEniCS. We solved this issue by first letting FEniCS assemble the matrix A and the right-side vector b without the π_h terms, and then assemble the π_h terms ourselves and update the matrix A and the vector b accordingly. It turns out that the π_h terms are not very difficult to assemble.

4 Numerical Results

The simulation setup is as in Figure 4. The reference domain is $[0, \text{AR}] \times [0, 1]$. The clamps constraint are imposed at $X = 0$ and $X = \text{AR}$. At the beginning, the elastomer is pre-stretched

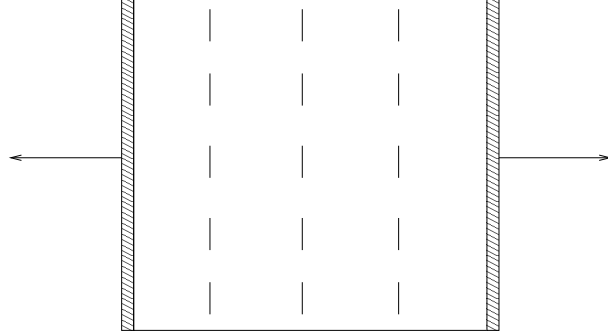


Figure 4: The elastomer is clamped and pulled on both sides.

to the stress-free state, and it's assumed that at this state the directors are aligned uniformly in the direction

$$\mathbf{n} = (0, 1)^T \quad (104)$$

The values of the displacement, pressure etc. at the stress-free state were mentioned in section 2.3. For completeness, we rewrite them here. The displacement at the stress-free state is given by

$$u_X = (a^{1/4} - 1)(X - 0.5\text{AR}) \quad (105)$$

$$u_Y = (a^{-1/4} - 1)(Y - 0.5) \quad (106)$$

The pressure at the stress-free state is given by

$$p = 2a^{1/2} \quad (107)$$

And λ at the stress-free state is given by

$$\lambda = (1 - a)/\sqrt{a} \quad (108)$$

Suppose we want the aspect ratio at the stress-free state to be AR_n , we need to set

$$\text{AR} = \frac{1}{\sqrt{a}} \text{AR}_n \quad (109)$$

Notice that the whole problem is symmetric about both the vertical middle line $X = 0.5\text{AR}$ and the horizontal middle line $Y = 0.5$. Hence we only need to do the computation at the upper-right quarter $[0.5\text{AR}, \text{AR}] \times [0.5, 1]$. By symmetry, we have the following Dirichlet boundary conditions:

$$u_X = 0 \quad \text{on } X = 0.5\text{AR} \quad (110)$$

$$u_Y = 0 \quad \text{on } Y = 0.5 \quad (111)$$

$$\mathbf{n} = (0, 1)^T \quad \text{on } X = 0.5\text{AR} \text{ and } Y = 0.5 \quad (112)$$

Also, we model the ‘‘clamped pulling’’ by specifying the following Dirichlet boundary conditions at $X = \text{AR}$:

$$u_X = 0.5\text{AR}[a^{1/4}(1 + Mt) - 1] \quad (113)$$

$$u_Y = (a^{-1/4} - 1)(Y - 0.5) \quad (114)$$

$$\mathbf{n} = (0, 1)^T \quad (115)$$

where $t \in [0, 1]$, and $1 + M$ is the largest elongation factor (ratio of the length of the elastomer after stretching and the length of the elastomer before the stretching). We slowly increases t from 0 to 1, to increase the numerical stability of the Newton's method. To make sure that $|\mathbf{n}| = 1$ at all the mesh nodes, we need to impose Dirichlet boundary conditions for λ at the *same* boundary as \mathbf{n} . Therefore we impose

$$\lambda = (1 - a)/\sqrt{a} \quad \text{on } X = 0.5AR, X = AR \text{ and } Y = 0.5. \quad (116)$$

We took $a = 0.6$, $b = 0.0015$, $AR_n = 1$, $M = 0.4$, with "time" step $\Delta t = 0.01$. We have used uniform triangular meshes in the simulations. For example, Figure 5 shows the mesh with mesh size $h = 2^{-5}$ (notice that the mesh is 16×16 , but recall that this computational domain is only $1/4$ of the true domain).

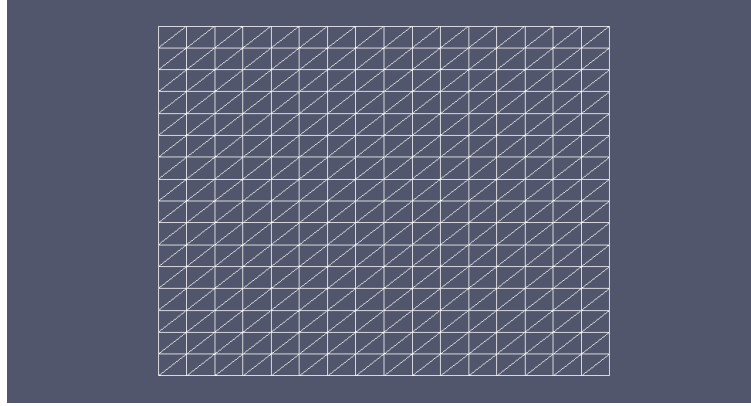


Figure 5: The uniform meshes we have used. What's shown here is the mesh with mesh size $h = 2^{-5}$.

Table 1 summarizes the numerical errors. We can see that the L^2 errors of \mathbf{u}_h and \mathbf{n}_h , and H^{-1} error of λ_h are relatively small, while the H^1 errors of \mathbf{u}_h and \mathbf{n}_h are relatively large. Table

h	2^{-2}	2^{-3}	2^{-4}	2^{-5}
$\ \mathbf{u}_h - \mathbf{u}_{h/2}\ _0$	3.49E-03	1.91E-03	8.39E-04	2.69E-04
$\ \mathbf{u}_h - \mathbf{u}_{h/2}\ _1$	5.14E-02	3.77E-02	2.02E-02	7.66E-03
$\ \mathbf{n}_h - \mathbf{n}_{h/2}\ _0$	2.32E-01	9.70E-02	3.05E-02	8.25E-03
$\ \mathbf{n}_h - \mathbf{n}_{h/2}\ _1$	2.31E+00	1.91E+00	1.19E+00	6.23E-01
$\ p_h - p_{h/2}\ _0$	1.68E-01	7.93E-02	2.38E-02	8.99E-03
$\ \lambda_h - \lambda_{h/2}\ _{-1}$	1.15E-02	4.41E-03	1.51E-03	5.22E-04

Table 1: The numerical errors.

2 summarizes the convergence rates. We can see that the convergence rates are relatively fast, except the H^1 errors of \mathbf{u}_h and \mathbf{n}_h .

Next, let's check the results of the inf-sup tests. Table 3 lists the inf-sup values at $t = 0$, where $s(\mathcal{A}|\text{Ker}(\mathcal{B}))$ is the inf-sup value of $\mathcal{A}|\text{Ker}(\mathcal{B})$, while $e(\mathcal{A}|\text{Ker}(\mathcal{B}))$ is the ellipticity constant of $\mathcal{A}|\text{Ker}(\mathcal{B})$. We can see that the inf-sup values of b_1 and b_2 don't change much with the mesh. This implies that the inf-sup conditions for b_1 and b_2 probably are always satisfied regardless of the mesh. Next, we can see that the inf-sup values for $s(\mathcal{A}|\text{Ker}(\mathcal{B}))$ are positive for all the 4 meshes, which means the inf-sup conditions are satisfied thus the discrete saddle point systems are well-posed for all the 4 meshes. However, it seems that the inf-sup values $s(\mathcal{A}|\text{Ker}(\mathcal{B}))$ tend to 0 as h goes to 0. Finally, we can see that the ellipticity constants $e(\mathcal{A}|\text{Ker}(\mathcal{B}))$ are negative for the given 4 meshes. This means the ellipticity conditions are not satisfied at the initial stress-free state. This is consistent with our analytical observation. Table 4 lists the inf-sup values at the

h	2^{-3}	2^{-4}	2^{-5}
$\log_2(\ \mathbf{u}_{2h} - \mathbf{u}_h\ _0 / \ \mathbf{u}_h - \mathbf{u}_{h/2}\ _0)$	0.87	1.18	1.64
$\log_2(\ \mathbf{u}_{2h} - \mathbf{u}_h\ _1 / \ \mathbf{u}_h - \mathbf{u}_{h/2}\ _1)$	0.45	0.90	1.40
$\log_2(\ \mathbf{n}_{2h} - \mathbf{n}_h\ _0 / \ \mathbf{n}_h - \mathbf{n}_{h/2}\ _0)$	1.26	1.67	1.88
$\log_2(\ \mathbf{n}_{2h} - \mathbf{n}_h\ _1 / \ \mathbf{n}_h - \mathbf{n}_{h/2}\ _1)$	0.27	0.69	0.93
$\log_2(\ p_{2h} - p_h\ _0 / \ p_h - p_{h/2}\ _0)$	1.08	1.74	1.41
$\log_2(\ \lambda_{2h} - \lambda_h\ _{-1} / \ \lambda_h - \lambda_{h/2}\ _{-1})$	1.38	1.55	1.54

Table 2: The convergence rates.

h	2^{-2}	2^{-3}	2^{-4}	2^{-5}
b_1	0.5836	0.5875	0.5879	0.5880
b_2	2.0000	2.0000	2.0000	2.0000
$s(\mathcal{A} \text{Ker}(\mathcal{B}))$	3.60E-03	2.70E-04	5.69E-05	1.62E-04
$e(\mathcal{A} \text{Ker}(\mathcal{B}))$	-3.60E-03	-1.27E-02	-1.78E-02	-1.21E-02

Table 3: The inf-sup values at $t = 0$.

final state $t = 1$ (elongation factor $s = 1.4$). We can see that the inf-sup values for b_1 and b_2 still don't vary much with respect to the mesh size h . This suggests that the inf-sup conditions for b_1 and b_2 are probably satisfied for all the \mathbf{u}_h and \mathbf{n}_h solutions during the pulling process. On the other hand, we still see that $s(\mathcal{A}|\text{Ker}(\mathcal{B}))$ are positive, while $e(\mathcal{A}|\text{Ker}(\mathcal{B}))$ are negative, which means the inf-sup condition for $s(\mathcal{A}|\text{Ker}(\mathcal{B}))$ are satisfied, while the ellipticity condition are not. Similar to $t = 0$, although the inf-sup values $s(\mathcal{A}|\text{Ker}(\mathcal{B}))$ are positive for the 4 given meshes, they do seem to converge to zero as the mesh size h goes to 0.

h	2^{-2}	2^{-3}	2^{-4}	2^{-5}
b_1	0.6549	0.6431	0.6287	0.6163
b_2	1.9967	1.9503	1.9065	1.8711
$s(\mathcal{A} \text{Ker}(\mathcal{B}))$	2.91E-03	1.20E-03	5.82E-04	4.88E-05
$e(\mathcal{A} \text{Ker}(\mathcal{B}))$	-2.91E-03	-2.58E-03	-5.82E-04	-4.88E-05

Table 4: The inf-sup values at $t = 1$.

Figure 6 shows the graph of nominal stress vs. strain, where we have taken the stress-free state as the reference configuration. We can clearly see a plateau when the strain is in $(0.10, 0.22)$. Comparing with Figure 2, we can say that we've recovered the semi-soft elasticity phenomenon. The plateau regions in Figure 2 are more flat than ours, because those graphs are for long and thin elastomers, while our graph is for the elastomer with the aspect ratio $\text{AR}_n = 1$.

Figure 7,8 and 9 show the directors configuration at the start, bottom, and end of the plateau region (elongation factor is about 1.10, 1.17 and 1.22 respectively). We can see that the directors just start to rotate at the start of the plateau region (Figure 7), while many of the directors have finished the rotations at the end of the plateau region (Figure 9). Also, we can see from Figure 7,8 and 9 that during the plateau interval $(0.10, 0.22)$, the elastomer domain is mostly blue (low BTW energy); while after the plateau region (Figure 10), the red part (high BTW energy) starts to dominate the elastomer domain. This means by rotating the directors, the elastomer maintains relatively low BTW energy during the elongation; while after most of the directors have already finished the rotation, the BTW energy starts to increase. This suggests that the plateau region in the stress-strain graph is probably caused by the rotation of the directors. This agrees with the theory of liquid crystal elastomers [19].

Figure 10 shows the final configuration of the directors (elongation factor $s = 1.4$). We can see that most of the directors have finished the rotation in the final state.

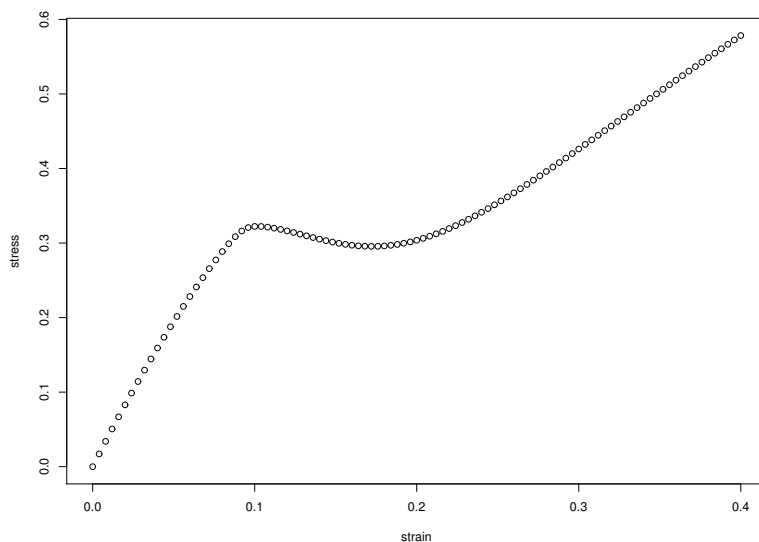


Figure 6: Nominal stress vs. strain. The plateau region corresponds to strains in the interval (0.10, 0.22).

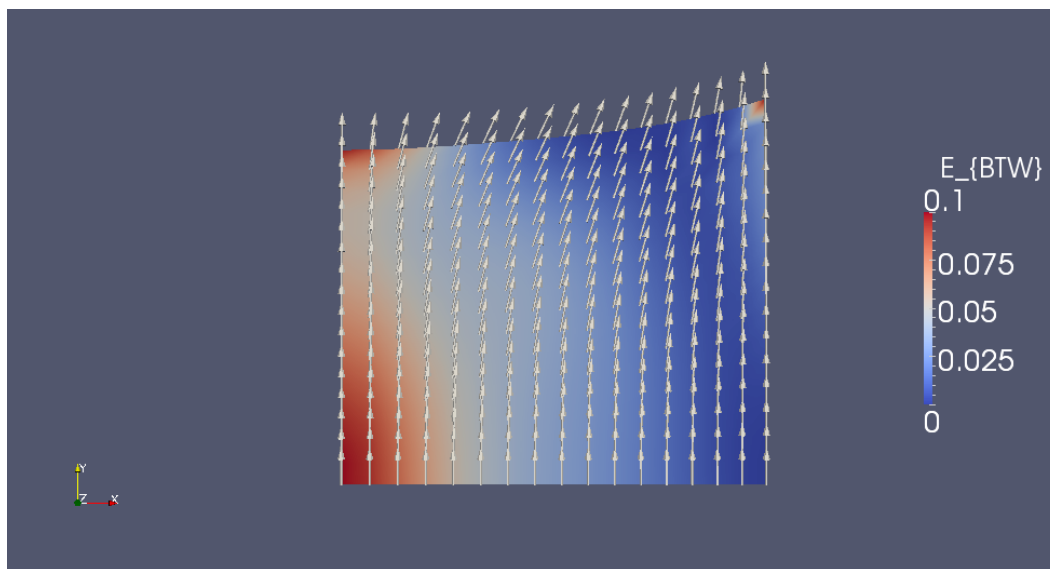


Figure 7: The directors at the beginning of the plateau region, elongation factor $s = 1.10$.

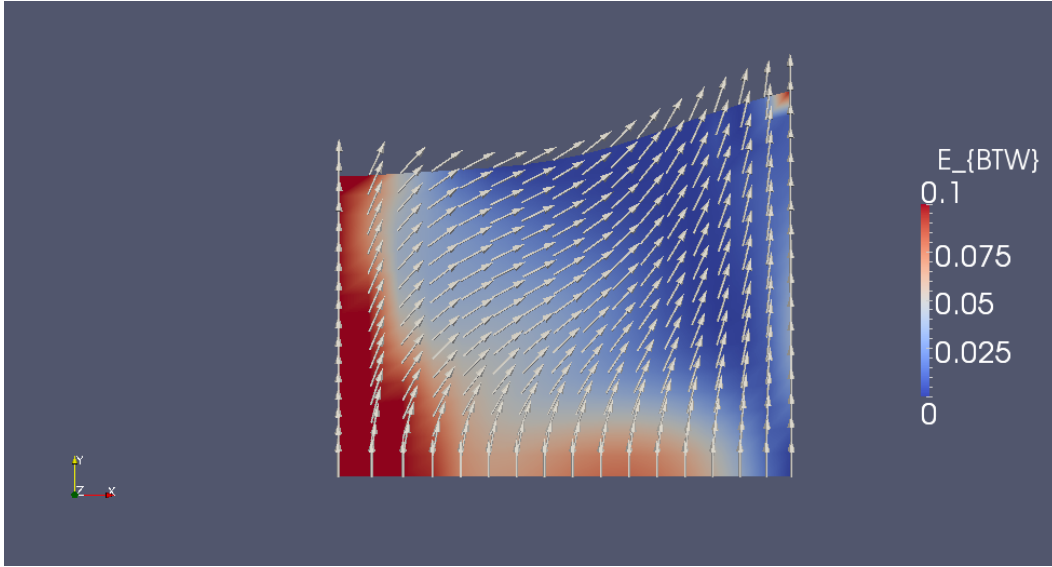


Figure 8: The directors at the bottom of the plateau region, elongation factor $s = 1.17$.

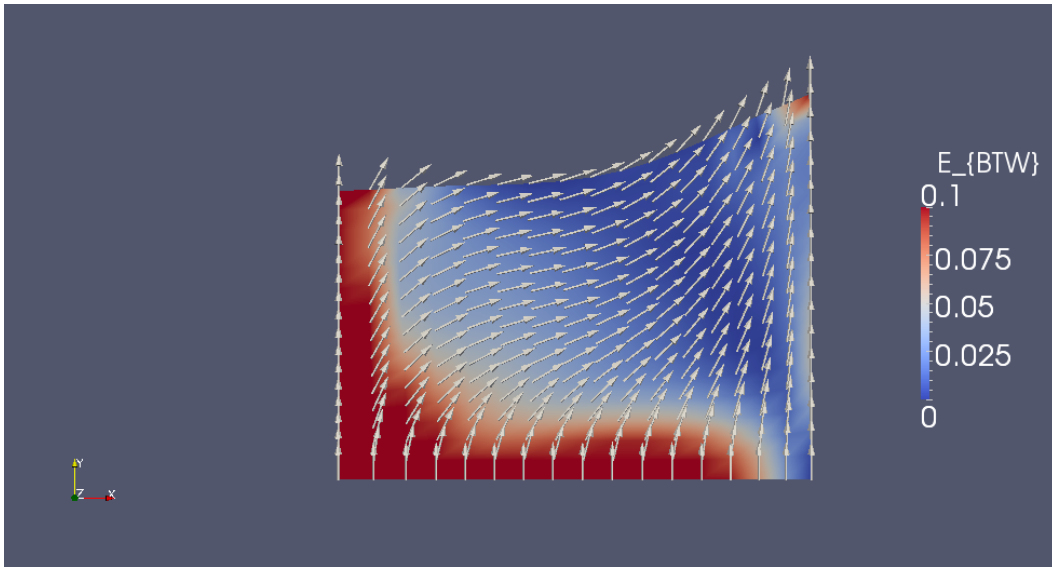


Figure 9: The directors at the end of the plateau region, elongation factor $s = 1.22$.

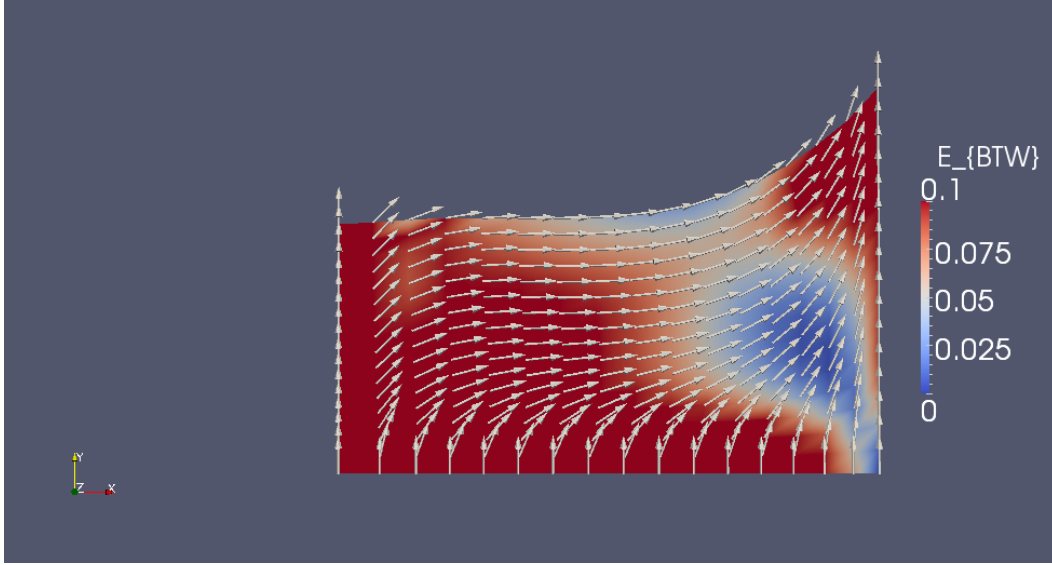


Figure 10: The directors at the final state, elongation factor $s = 1.4$.

5 Conclusion and Discussion

We have designed a numerical algorithm to simulate the 2D BTW+Oseen-Frank model of liquid crystal elastomer. We aimed to recover numerically the experimentally observed phenomena such as the stripe-domain phenomenon, the semi-soft elasticity etc. The existence, well-posedness, uniqueness and convergence etc. of the numerical algorithm have been investigated.

We have successfully captured the semi-soft elasticity of liquid crystal elastomer, and found it to be related with the rotation of the directors. However, we didn't see the stripe-domain phenomenon. We believe this is mainly because the b value (the coefficient of the Oseen-Frank energy) 0.0015 is relatively large comparing to true value of b in practice, which we estimate to be probably less than 10^{-6} . Since the b value is relatively large, the Oseen-Frank energy dominates the BTW energy, while the latter of which is the main driving force for the occurrence of stripe domains. On the other hand, to observe the stripe domain phenomenon, we should use meshes fine enough to resolve the stripes. For example, in the experiment of Zubarev and Finkelmann ([20]), the width of stripe domain divided by the width of the elastomer is around $15\mu\text{m}/5\text{mm} = 0.003$, which is much smaller than the mesh size 2^{-5} of our finest mesh. However, very small b values require small "time" steps to be stable, and this together with very fine meshes would be computationally very expensive. We have tried 512×512 uniform mesh, and the program ran out of memory. In the future, when the machines have much greater computing power, we can try very small b values and very fine mesh, and see whether the stripe domain occurs. Instead of using uniformly fine mesh, we can also use adaptive mesh to reduce the computational cost.

Another direction worth trying is to use Ericksen or Landau-de Gennes' model instead of the Oseen-Frank energy in the numerical simulation. Oseen-Frank energy only allows point defects, while Ericksen or Landau-de Gennes' model allows line and surface defects, as well ([16]). The stripe domains might have line or surface defects in the transition area between the stripes, thus using Ericksen or Landau-de Gennes' model might have a better chance of capturing the stripe domain phenomenon.

References

- [1] J. BALL, *Convexity conditions and existence theorems in nonlinear elasticity*, Archive for rational mechanics and Analysis, 63 (1976), pp. 337–403.

- [2] P. BLADON, E. TERENTJEV, AND M. WARNER, *Transitions and instabilities in liquid crystal elastomers*, Physical Review E, 47 (1993), pp. 3838–3840.
- [3] F. BREZZI AND M. FORTIN, *Mixed and Hybrid Finite Element Methods*, Springer, Berlin, 1991.
- [4] P. CIARLET, *Mathematical Elasticity, Vol 1*, North-Holland, 1987.
- [5] F. CLARKE, *Generalized gradients and applications*, Transactions of the American Mathematical Society, 205 (1975), pp. 247–262.
- [6] ———, *A new approach to Lagrange multipliers*, Mathematics of Operations Research, 1 (1976), pp. 165–174.
- [7] S. CLARKE, A. HOTTA, A. TAJBAKSHI, AND E. TERENTJEV, *Effect of crosslinker geometry on equilibrium thermal and mechanical properties of nematic elastomers*, Physical Review E, 64 (2001), p. 61702.
- [8] S. CONTI, A. DESIMONE, AND G. DOLZMANN, *Soft elastic response of stretched sheets of nematic elastomers: a numerical study*, Journal of the Mechanics and Physics of Solids, 50 (2002), pp. 1431–1451.
- [9] L. EVANS, *Partial Differential Equations*, American Mathematical Society, (1998).
- [10] FENICS, *FEniCS project*. URL: [urlhttp://www.fenics.org/](http://www.fenics.org/).
- [11] F. FRANK, *I. Liquid crystals. On the theory of liquid crystals*, Discussions of the Faraday Society, 25 (1958), pp. 19–28.
- [12] Q. HU, X. TAI, AND R. WINTHER, *A saddle point approach to the computation of harmonic maps*, SIAM Journal on Numerical Analysis, 47 (2009), pp. 1500–1523.
- [13] I. KUNDLER AND H. FINKELMANN, *Strain-induced director reorientation in nematic liquid single crystal elastomers*, Macromolecular rapid communications, 16 (1995), pp. 679–686.
- [14] J. KÜPPER AND H. FINKELMANN, *Liquid crystal elastomers: influence of the orientational distribution of the crosslinks on the phase behaviour and reorientation processes*, Macromolecular chemistry and physics, 195 (1994), pp. 1353–1367.
- [15] P. LE TALLEC, *Compatibility condition and existence results in discrete finite incompressible elasticity*, Computer Methods in Applied Mechanics and Engineering, 27 (1981), pp. 239–259.
- [16] A. MAJUMDAR AND A. ZARNESCU, *Landau–De Gennes Theory of Nematic Liquid Crystals: the Oseen–Frank Limit and Beyond*, Archive for rational mechanics and analysis, 196 (2010), pp. 227–280.
- [17] G. MITCHELL, F. DAVIS, AND W. GUO, *Strain-induced transitions in liquid-crystal elastomers*, Physical review letters, 71 (1993), pp. 2947–2950.
- [18] P. L. TALLEC, *Numerical methods for nonlinear three-dimensional elasticity*, Handbook of Numerical Analysis, 3 (1994), pp. 465–622.
- [19] M. WARNER AND E. TERENTJEV, *Liquid crystal elastomers*, Oxford University Press, USA, 2007.
- [20] E. ZUBAREV, S. KUPTSOV, T. YURANOVA, R. TALROZE, AND H. FINKELMANN, *Monodomain liquid crystalline networks: reorientation mechanism from uniform to stripe domains*, Liquid crystals, 26 (1999), pp. 1531–1540.